Qutip-lattice: A python package for topology and transformation problems defined on lattice

Saumya Biswas and Avik Dutt*
Department of Mechanical Engineering, University of Maryland, College Park, MD 20742, USA

Amrit De
Department of Electrical Engineering, University of California - Riverside, CA 92521, USA

Clemens Gneiting and Franco Nori†
Theoretical Quantum Physics Laboratory, RIKEN Cluster for Pioneering Research, Wako-shi, Saitama 351-0198, Japan
and
RIKEN Center for Quantum Computing, Wako-shi, Saitama 351-0198, Japan

Eric Giguére
Universit de Sherbrooke
(Dated: December 15, 2022)

I. INTRODUCTION

Lattice models are of fundamental interest in physics. From gauge theories defined on lattices to tight-binding models embodying effective theories, the reach and manifestation of lattice models are all-pervasive. QuTiP is an open source python software package especially for simulating open system dynamics problems in quantum optics [1]. The versatilities of the capabilities of QuTiP with open system dynamics are amenable to integration with widely used lattice models with legacies of their own. The single particle physics, while numerically less demanding suffice for the explanation of a vast treasure trove of physics encompassing problems of topological phases of matter, excitation spectra and transport properties. Many particle models, on the other hand, are numerically burdensome and require clever techniques of symmetry transformations for making computations feasible. Qutip-lattice package offers the famous many-particle physics Hubbard models implementations in bases of symmetry with manageable computational load. A few fermionic and bosonic models and interesting transformation properties are included. Some well konwn transformations useful for diagonalization calculations, the calculation of the ground state and excitation spectra are offered. Some Non-Hermitian Hamiltonian(NHH) models which are driving new avenues of research can also be investigated. Many-body physics of atoms and light [2] and models embodying gain and loss mechanism [3] are of special interest.

Notable among exisitng open source packages for lattice dynamics problems is QuSpin [4, 5], which is exact diagonalization based. qutip-lattice offers some of the functionalities covered in QuSpin and more on topology and non-Hermitian models. The ALPS project is a distant fore-runner for stronly correlated physics [6], with support for modern approximate methods of Matrix Product States(MPS) and Density Matrix Renormalization Group (DMRG)[7]. Among python based DMRG softwares for lattice models Quimb is noteworthy [8].

II. THEORY OF BASIS SYMMETRIZATION

Symmetries are our silver bullet for demystifying the maze of natural laws. Symmetries dictate the conservation laws, creates the degeneracies, define the structure of matter and interacrtions. Symmetry can disintegrate evolution of matter and energy into disjoint fundamental subprocesses making their computation not only easier but also possible. Choice of the computational basis $|c_i\rangle$ helps enumerate a tractable basis for the problem as well as help codify the Hamiltonian into a matrix form $\langle c_i|\hat{H}|c_j\rangle$ in the spirit of Heisenberg's matrix formulation of quantum mechanics.

The symmetrized basis according to translational symmetry group, TG stands,[9]

$$|\tilde{c}\rangle = \frac{1}{N(c,k)} \sum_{t \in TG} \chi(t)^k |(t)c\rangle, \tag{1}$$

* Also at Institute for Physical Science and Technology, University of Maryland, College Park, MD 20742, USA

† Also at Department of Physics, University of Michigan, Ann Arbor, Michigan 48109-1040, USA

where χ is the character of the symmetry transformation, N is the normalization constant, k is the wave-vector.

projection of the original Hilbert space onto an invariant subspace that corresponds to a particular irreducible representations of the symmetry group of the system G.

From the famous result from binomial theorem,

$$\binom{L}{0}+\binom{L}{1}+\binom{L}{2}+....+\binom{L}{(L-1)}+\binom{L}{L}=2^L \quad (2)$$

Since, $\binom{L}{0}=\binom{L}{L}=1$,

$$2+\sum_{2}^{L-1}\binom{L}{N}=2^L \quad (3)$$

The cue to the trick of compartmentalization or decomposition can be found in the eq. 3. In fact, for $spin-\frac{1}{2}$ chains, eq. 2 is applicable most conspicuously, as we shall be reminded later in this section. Decompsoitions like this is facilitated by the powerful concept of equivalnece classes.

Periodic boundary conditions also facilitate some classification into equivalence classes that is reminescent of Fermat's little theorem, as was noted in [10].

$$2+qN=2^L \quad (4)$$

In the context of spin-$\frac{1}{2}$ chains, the 2 in eqs. 3 and 4 are both accounting for all spin-up ($|+++...+++\rangle$) or spin-down ($|---...--\rangle$) configurations. These two spin configurations are the equivalence classes themselves. All other configurations are amenable to decompositions.

III. A PRIMER ON TRANSLATIONAL SYMMETRY

The periodic repitition of the unit cell in lattice models with periodic boundary condition make translational symmetry a powerful tool in lattice dynamics for problems preserving translational symmetry.

For the prototypical XXZ model [11],

$$\hat{H}=-\frac{J}{2}\sum_{l=0}^{L-1}\left[\hat{\sigma}_l^x\hat{\sigma}_{l+1}^x+\hat{\sigma}_l^y\hat{\sigma}_{l+1}^y+\Delta\hat{\sigma}_l^z\hat{\sigma}_{l+1}^z\right] \quad (5)$$

$$=-J\sum_{l=0}^{L-1}\left[\hat{\sigma}_l^+\hat{\sigma}_{l+1}^-+\hat{\sigma}_l^-\hat{\sigma}_{l+1}^++\frac{\Delta}{2}\hat{\sigma}_l^z\hat{\sigma}_{l+1}^z\right] \quad (6)$$

A complete basis is facilitated by the spin tensor basis $|\vec{S}_0\otimes\vec{S}_1\otimes\vec{S}_2\otimes....\vec{S}_{L-1}\rangle$ [12]. The spins are all 'good quantum numbers' i.e. can be used to label the complete set of eigenstates. Spin-$\frac{1}{2}$ systems are most commonly represented in the S^z computational basis [9].

$$|\uparrow\uparrow\downarrow\uparrow\rangle\rightarrow|1101\rangle \quad (7)$$

In the S_z-basis, the basis vectors are the tensor product os the S_z-components of the L spins [12],

$$|u_i\rangle=|S_1S_2S_3....S_{L-1}S_L\rangle$$

The translation operator $\hat{T}$ shifts the spins by mapping $|u_i\rangle$ to a different $|u_j\rangle$ with the spins shifted by one (notation of [13]).

$$\hat{T}|u_i\rangle=\hat{T}|S_1S_2S_3....S_{L-1}S_L\rangle$$
$$=|S_LS_1S_2S_3....S_{L-1}\rangle=|u_j\rangle \quad (8)$$

We use two definitions from [9]. Definition 1. Two vectors $|u_i\rangle$ and $|u_j\rangle$ are translationally related if $\hat{T}^n|u_i\rangle=|v_i\rangle$ for some integer $n\leq N$.

Definition 2. A set of m translationally related vectors $\{|u_1\rangle,|u_2\rangle,,|u_k\rangle,,|u_m\rangle\}$ such that for any member $|u_k\rangle$, the relationship $\hat{T}^m|u_k\rangle=|u_k\rangle$ holds is called a cycle of period m.

Since, $\hat{T}^n|u_i\rangle=|v_i\rangle$ is an equivalence relation, and as such it can induce a complete decomposition of the basis into disjoint subsets or equivalence classes. A 'cycle' is defined to be the linear span of such an equivalence class of basis vectors. A cycle with a period of N is called a 'proper cycle', and smaller period cycle are called 'epicycles' in the notation of [13].

If $|\psi_r\rangle$ is one of the m (the period) primary basis states of a cycle (in qutip.lattice() the lowest binary number is picked as the representative), it can be chosen as the representative of the cycle,

$$|\psi_r\rangle=|m_1,m_2,m_3,....m_x,..,m_N\rangle \quad (9)$$

The rest of the cycles in the equivalence class can be enumerated as,

$$|\psi_n\rangle=\hat{T}^n|\psi_r\rangle,\quad n=1,...,m \quad (10)$$

The cycle is spanned by

$$|\chi_k\rangle=\frac{\sqrt{m}}{L}\sum_{l=0}^{L-1}\omega_k^{-l}\hat{T}^l|\psi_r\rangle \quad (11)$$

which is an eigenstate of $\hat{T}$ with quasi-momentum (called 'magnon momentum' in spin problems) $\frac{2\pi k}{N}$.

Ref. [12] reminds us of the decomposition relations talked about in eq.s 3 and 4. with the formal result,

$$\sum(\text{dimension}\times\text{number of cycles})=2^L \quad (12)$$

For m prime and L=m, with X(m) being the number of dimension m cycle,

$$1\times2+m\times X(m)=2^m \quad (13)$$

A. Excitation/Number Symmetry

Since, the number operator commutes with both $\mathcal{H}$, the equivalence class/ orthogonal subgroup direct product of the Hilbert space can be done into subgroups of fixed excitation numbers as well.

$$H=H_{N=0}\oplus H_{N=1}\oplus...\oplus H_{N=n}\oplus...\oplus H_{N=L-1} \quad (14)$$

For a lattice of spin-$\frac{1}{2}$s, the Hilbert space dimension of H_N is easy to compute, $\binom{N}{n}$. Formulae for more general lattices (other spins and space dependent spins) can be found in [13].

On top of that, since, the number operator commutes with both $\mathcal{H}$ and $\hat{T}$, the direct product decomposition can also be with the combined symmetries,

$$H_{N=N} = H_{N,k=0} \oplus H_{N,k=1} \oplus H_{N,k=2} \oplus ... \oplus H_{N,k=L-1} \quad (15)$$

The Hilbert space of H is the direct sum of all the eigenspace of $H_{N,k}$. Naming the represtative basis state $|n\rangle$, the action of the shift operator, $\hat{T}$ can be written as,

$$\hat{T}|n\rangle = |T(n)\rangle, \quad (16)$$

where the function $T(n)$ shifts binary bits by a unit distance. Since $\hat{T}^L = 1$, $\hat{T}$ has the eigenvalue,

$$\omega_k = \exp\left(\frac{2\pi i k}{L}\right), \quad (k = 0, 1, 2, ...L-1) \quad (17)$$

Since, the Hamiltonian is invariant under spin translations i.e. $\left[\mathcal{H}, \hat{T}\right] = 0$, it can be block-diagonalized in the simultaneous eigenstates of $\mathcal{H}$ and $\hat{T}$. The simultaneous eigenstate of $\hat{N}$ and $\hat{T}$ with eigenvalue N and ω_k respectively are,

$$|\bar{n}, k\rangle = \frac{\sqrt{p(\bar{n})}}{L} \sum_{l=0}^{L-1} \omega_k^{-l} \hat{T}^l |\bar{n}\rangle \quad (18)$$

with

$$kp(\bar{n}) = integer \times L \quad (19)$$

This condition can alternately be constructed as,

$$\sum_{l=1}^{N} e^{ikl/L} \neq 0 \quad (20)$$

i.e. sum of the phase aquired as the basis representative vector as it is translated one site at a time must not sum to zero. If it is zero, then it is not a cycle and in fact does not have a period.

IV. CANONICAL TRANSFORMATIONS

A mixture of analytic/semi-analytic transformations are available for diagonalization of lattice Hamiltonians[14].

V. SINGLE PARTICLE PHYSICS

Single particle models confine its scope to single excitation manifold alone. A number of experiments are explainable with single particle models only. The disperion relation, quantum transport models, certain topological phases of matter are accurately described by single particle physics models. Lattice1d() class in qutip.lattice facilitates defining and simulating single particle physics problems.

$$|\psi_n(k)\rangle = |k\rangle \otimes |u_n(k)\rangle$$
$$|u_n(k)\rangle = a_n(k)|a\rangle + b_n(k)|b\rangle \quad (21)$$

The vectors $|u_{nk}(r)\rangle \in H_{internal}$ are the eigenstates of the bulk momentum space Hamiltonian $H(k)$ defined as

$$\langle k|H_{bulk}|k\rangle = \sum_{\alpha,\beta \in A,B} \langle k, \alpha|H_{bulk}|k, \beta\rangle |\alpha\rangle\langle\beta|$$
$$H(k)|u_n(k)\rangle = E(k)|u_n(k)\rangle \quad (22)$$

In a lattice with N unitcells, since $|\psi_n(k)\rangle$ is required to be periodic over N cells, it needs to be invariant with a translation by N cells, and the valid/good quantum number for k are $0, 1, 2, ..., \frac{2\pi}{N}$.

```
from qutip import *
import matplotlib.pyplot as plt
import numpy as np
```

Listing 1. Python example

A. Lattice1d examples: SSH model: dispersion, winding number, edge modes

SSH model is a paradigmic model in topological quantum theory [15]. Hence, H_{TB} can be succinctly put in the form:

$$H_{per/aper} = \sum_i \psi_i^\dagger D \psi_i + \sum_i \left(\psi_i^\dagger T \psi_{i+1} + \psi_{i+1}^\dagger T^\dagger \psi_i\right) \quad (23)$$

where $D = \begin{bmatrix} 0 & -t_{intra} \\ -t_{intra} & 0 \end{bmatrix}$ and $T = \begin{bmatrix} 0 & 0 \\ -t_{inter} & 0 \end{bmatrix}$. The $\psi_i = \begin{bmatrix} c_i^0 \\ c_i^1 \end{bmatrix}$ is associated with $\vec{R} = \vec{R}_i$ and ψ_{i+1} is associated with $\vec{R} = \vec{R}_i + \hat{x}$, with $\hat{x}$ being the unit vector along the x direction.

The equation above can be put into the alternate form (also changing the summation variables to m,n to distinguish them from the imaginary i):

$$H_{per/aper} = \sum_{m,n} \psi_m^\dagger (D\delta_{m,n} + T\delta_{m,n-1} + T^\dagger \delta_{m,n+1}) \psi_n \quad (24)$$

Due to the chiral symmetry, the bulk momentum space Hamiltonian,$H(k)$ can be written in terms of σ_x and σ_y components alone.

$$H(k) = h_x(k)\sigma_x + h_y(k)\sigma_y \quad (25)$$

For this specific model, where $\mathbf{h}(\mathbf{k})$ moves about in a 2d plane($h_x - h_y$), winding number is a topological invariant characterizing the topology of the model. It enumerates the number of times, $\mathbf{h}(\mathbf{k})$ traverses around the origin in a positive sense as k is varied from 0 to 2π. The method $winding_number()$ evaluates the following integral to determine it as well as plots the trajectory of $\mathbf{h}(\mathbf{k})$ in the $h_x - h_y$ plane.

$$\nu = \frac{1}{2\pi i}\int_{-\pi}^{\pi} dk \frac{d}{dk} Log(h(k))$$
$$\text{,where} \qquad h(k) = h_x(k) - ih_y(k) \tag{26}$$

```
t_intra = -0.5
t_inter = -0.5
H_cell[0,1] = t_intra
H_cell[1,0] = t_intra
T_inter_cell[1,0] = t_inter
H_cell = Qobj(H_cell)
T_inter_cell = Qobj(T_inter_cell)
H_cell = Qobj( np.array( [[ 0, t_intra ],[
    t_intra,0]]))
T_inter_cell =  Qobj( np.array( [[ 0, 0 ],[
    t_inter,0]]))
```

Listing 2. Python example

```
boundary_condition = "periodic"
cells = 3
cell_sites = 2
site_dof = [1]
SSH_lattice = Lattice1d(num_cell=cells, boundary
     = boundary_condition, cell_num_site =
    cell_sites, cell_site_dof = site_dof,
    Hamiltonian_of_cell = H_cell, inter_hop =
    T_inter_cell )
```

Listing 3. Python example

```
t_intra = -0.5
t_inter = -0.65
cell_H = Qobj( np.array( [[ 0, t_intra ],[
    t_intra,0]] )  )
inter_cell_T =  Qobj( np.array( [[ 0, 0 ],[
    t_inter,0]] )  )
apSSH_lattice_nTrI = Lattice1d(num_cell=100,
    boundary = "aperiodic", cell_num_site = 2,
    cell_site_dof = [1], Hamiltonian_of_cell =
    cell_H, inter_hop = inter_cell_T )
```

Listing 4. Python example

```
pSSH_lattice_nTrI.plot_dispersion()
```

Listing 5. Python example

The midgap states do not appear in the Periodic Boundary Condition case.

```
In[1]: apSSH_lattice_nTrI.winding_number()
Out[1]: 1
```

Listing 6. Python example

```
apSSH_H_nt = apSSH_lattice_nTrI.Hamiltonian()
[n_D,Vx] = apSSH_H_nt.eigenstates()
```

Listing 7. Python example

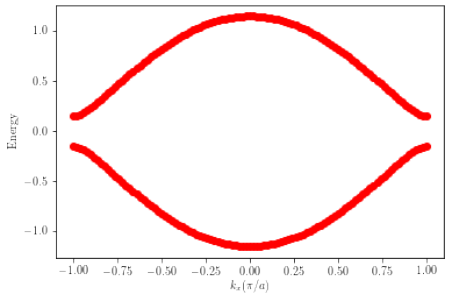

FIG. 1. Dispersion of SSH model.

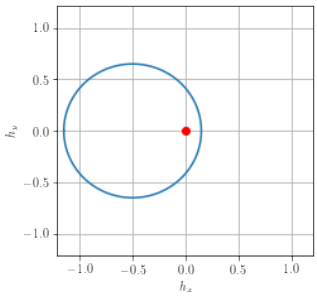

FIG. 2. Contour of h(k).

```
plt.plot(n_D,'ro')
plt.ylabel('eigen values')
plt.show()
plt.close()
```

Listing 8. Python example

Open Boundary Condition reveals the midgap edge states.

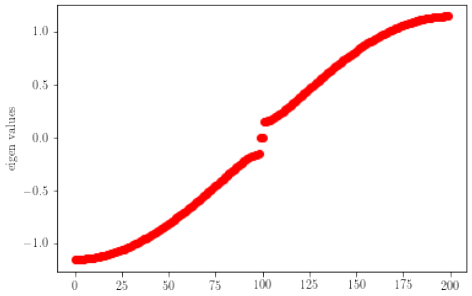

FIG. 3. Eigenvalues of the SSH lattice Hamiltonian.

VI. MANY PARTICLE PHYSICS MODELS

A. Normal Ordering

We follow the notation from [16]. Fermionic wavefunctions are written out in the basis with a fixed number of particles, $N = N_\uparrow + N_\downarrow$

$$|\Psi_F\rangle = \sum_{x,y} w_F(x,y)|\mathbf{x},\mathbf{y}\rangle_{\mathbf{F}} \tag{27}$$

Here, $\mathbf{x} = (\mathbf{x_1}, \mathbf{x_2}, ..., \mathbf{x_{N_\uparrow}})$ and $\mathbf{y} = (\mathbf{y_1}, \mathbf{y_2}, ..., \mathbf{y_{N_\downarrow}})$ indicate the sites occupied respectively by the spin-up and spin-down ($spin - \frac{1}{2}$) fermions and $x_i \neq x_j, y_i \neq y_j \forall i, j$. Basis states are normal ordered. The definition is,

$$|x,y\rangle_F = f^\dagger_{x_1,\uparrow} f^\dagger_{x_2,\uparrow} .... f^\dagger_{x_{N_\uparrow},\uparrow} f^\dagger_{y_1,\downarrow} f^\dagger_{y_2,\downarrow} .... f^\dagger_{y_{N_\downarrow},\downarrow} |vac\rangle \tag{28}$$

$$\tag{29}$$

So, the down-spin creation operators act first in the order of decreasing positional index, then the up-spin creation operators in the same style.

The off-diagonal elements arising from the Hamiltonian nearest neighbour hopping term $(-t) f^\dagger_{x_a,\uparrow} f_{x_{a+1},\uparrow}$ is nonzero only between,

$${}_F\langle x^f, y^f| = \langle vac| f_{y_{N_\downarrow},\downarrow} .... f_{y_2,\downarrow} f_{y_1,\downarrow} f_{x_{N_\uparrow},\uparrow} .. f_{x_a,\uparrow} .. f_{x_2,\uparrow} f_{x_1,\uparrow}$$

and

$$|x,y\rangle_F = f^\dagger_{x_1,\uparrow} f^\dagger_{x_2,\uparrow} .. f^\dagger_{x_{a+1},\uparrow} .. f^\dagger_{x_{N_\uparrow},\uparrow} f^\dagger_{y_1,\downarrow} f^\dagger_{y_2,\downarrow} .... f^\dagger_{y_{N_\downarrow},\downarrow} |vac\rangle$$

i.e. they would have all the same spin occupied positions except for x_a and x_{a+1}. Only $\langle x^f, y^f|$ will have x_a and only $|x,y\rangle$ will have x_{a+1}.

$$\begin{aligned}
&\langle vac| f_{y^f_{N_\downarrow},\downarrow} ..... f_{y^f_2,\downarrow} f_{y^f_1,\downarrow} f_{x^f_{N_\uparrow},\uparrow} .. f_{x^f_a,\uparrow} ... f_{x^f_2,\uparrow} f_{x^f_1,\uparrow} \\
&(-t) f^\dagger_{x_a,\uparrow} f_{x_{a+1},\uparrow} \\
&f^\dagger_{x_1,\uparrow} f^\dagger_{x_2,\uparrow} .. f^\dagger_{x_{a+1},\uparrow} .. f^\dagger_{x_{N_\uparrow}} f^\dagger_{y_1,\downarrow} f^\dagger_{y_2,\downarrow} .. \\
&.. f^\dagger_{y_{N_\downarrow}} |vac\rangle \\
&= (-1)^a \langle vac| f_{y^f_{N_\downarrow},\downarrow} ... \\
&... f_{y^f_2,\downarrow} f_{y^f_1,\downarrow} f_{x^f_{N_\uparrow},\uparrow} .. f_{x^f_a,\uparrow} ... f_{x^f_2,\uparrow} f_{x^f_1,\uparrow} \\
&(-t) f^\dagger_{x_a,\uparrow} \\
&f^\dagger_{x_1,\uparrow} f^\dagger_{x_2,\uparrow} .. f_{x_{a+1},\uparrow} f^\dagger_{x_{a+1},\uparrow} .. f^\dagger_{x_{N_\uparrow}} f^\dagger_{y_1,\downarrow} f^\dagger_{y_2,\downarrow} .... f^\dagger_{y_{N_\downarrow}} |vac\rangle \\
&= (-1)^a \langle vac| f_{y^f_{N_\downarrow},\downarrow} .. \\
&.... f_{y^f_2,\downarrow} f_{y^f_1,\downarrow} f_{x^f_{N_\uparrow},\uparrow} ... \\
&... f_{x^f_a,\uparrow} ... f_{x^f_2,\uparrow} f_{x^f_1,\uparrow} \\
&(-t) f^\dagger_{x_a,\uparrow} \qquad f^\dagger_{x_1,\uparrow} f^\dagger_{x_2,\uparrow} .. \left(1 - f^\dagger_{x_{a+1},\uparrow} f_{x_{a+1},\uparrow}\right) .. \\
&... f^\dagger_{x_{N_\uparrow}} f^\dagger_{y_1,\downarrow} f^\dagger_{y_2,\downarrow} .... f^\dagger_{y_{N_\downarrow}} |vac\rangle \\
&= (-1)^{2a} \langle vac| f_{y^f_{N_\downarrow},\downarrow} ... \\
&... f_{y^f_2,\downarrow} f_{y^f_1,\downarrow} f_{x^f_{N_\uparrow},\uparrow} .. f_{x^f_a,\uparrow} ... \\
&.... f_{x^f_2,\uparrow} f_{x^f_1,\uparrow} \qquad (-t) \qquad f^\dagger_{x_1,\uparrow} f^\dagger_{x_2,\uparrow} ... \\
&.... f^\dagger_{x_a,\uparrow} \left(1 - f^\dagger_{x_{a+1},\uparrow} f_{x_{a+1},\uparrow}\right) .. f^\dagger_{x_{N_\uparrow}} f^\dagger_{y_1,\downarrow} f^\dagger_{y_2,\downarrow} .... f^\dagger_{y_{N_\downarrow}} |vac\rangle \\
&= \langle vac| f_{y^f_{N_\downarrow},\downarrow} ..... f_{y^f_2,\downarrow} f_{y^f_1,\downarrow} f_{x^f_{N_\uparrow},\uparrow} .. f_{x^f_a,\uparrow} .... \\
&..... f_{x^f_2,\uparrow} f_{x^f_1,\uparrow} \qquad (-t) \qquad f^\dagger_{x_1,\uparrow} f^\dagger_{x_2,\uparrow} .... \\
&..... f^\dagger_{x_a,\uparrow} .. f^\dagger_{x_{N_\uparrow}} f^\dagger_{y_1,\downarrow} f^\dagger_{y_2,\downarrow} .... f^\dagger_{y_{N_\downarrow}} |vac\rangle = (-t)
\end{aligned}$$

In deriving the above, $f_{x_{a+1},\uparrow} f^\dagger_{x_{a+1},\uparrow} = \{f_{x_{a+1},\uparrow}, f^\dagger_{x_{a+1},\uparrow}\} - f^\dagger_{x_{a+1},\uparrow} f_{x_{a+1},\uparrow}$ was used.

B. Models

1. Extended Fermi Hubbard model

$$\begin{aligned}
H = &\sum_{j,\sigma} (\epsilon - \mu) c^\dagger_{j,\sigma} c_{j,\sigma} + \sum_{\langle j,k\rangle,\sigma} t_{j,k} c^\dagger_{j,\sigma} c_{k,\sigma} \\
&+ U \sum_j c^\dagger_{j,\uparrow} c^\dagger_{j,\downarrow} c_{j,\downarrow} c_{j,\uparrow} + V \sum_{\langle j,k\rangle,\sigma} c^\dagger_{j,\uparrow} c^\dagger_{j,\downarrow} c_{k,\downarrow} c_{k,\uparrow}
\end{aligned} \tag{30}$$

where c_i is the fermionic annihilation operator, $t_{j,k}$ is the nearest neighbour hopping.

```
num_sites = 4
fermiHubbardLattice1d = Lattice1d_fermi_Hubbard(
    num_sites=num_sites, boundary="periodic", t
    =1, U=1, V=2)
[Hamiltonian, basisReprUp, DownStatesPerRepr,
    normHubbardStates] = fermiHubbardLattice1d.
    Hamiltonian(fillingUp=2, fillingDown=2, kval
    =0)
```

Listing 9. Python example

2. Bose Hubbard model

$$\begin{aligned}
H = &\sum_j (\epsilon - \mu) b^\dagger_j b_j + \sum_{\langle j,k\rangle} t_{j,k} b^\dagger_j b_k \\
&+ U \sum_j \left(b^\dagger_j b_j b^\dagger_j b_j - b^\dagger_j b_j\right)
\end{aligned} \tag{31}$$

where b_i is the bosonic annihilation operator, $t_{j,k}$ is the nearest neighbour hopping.

```
num_sites = 4
Nmax=3
boseHubbardLattice1d = Lattice1d_bose_Hubbard(
    num_sites=num_sites, boundary="periodic", t
    =1, U=1)
[Hamiltonian, bosonbasis] = boseHubbardLattice1d
    .Hamiltonian(Nmax=Nmax, filling=2, kval=0)
```

Listing 10. Python example

3. *Two component Bose Hubbard model*

$$\hat{H} = \hat{H}_0 + \frac{U}{2}\sum_j \hat{n}_j\left(\hat{n}_j - 1\right)$$
$$\hat{H}_0 = \sum_{j\in odd}\left(t_1\hat{a}_j^\dagger\hat{a}_{j+1} + h.c.\right) + \sum_{j\in even}\left(t_2\hat{a}_j^\dagger\hat{a}_{j+1} + h.c.\right) + \sum_{j\in odd}\mu_A\hat{n}_j + \sum_{j\in even}\mu_B\hat{n}_j, \quad (32)$$

where a_i is the bosonic annihilation operator, $t_{1(2)}$ is the nearest neighbour hopping.

```
num_sites = 4
bose2cHubbardLattice1d =
    Lattice1d_2c_hcb_Hubbard(num_sites=num_sites
    , boundary="periodic", t=1, Uab=1)
[Hamiltonian, basisReprUp, DownStatesPerRepr,
    normHubbardStates] = bose2cHubbardLattice1d.
    Hamiltonian(fillingUp=2, fillingDown=2, kval
    =0)
```

Listing 11. Python example

4. *Hardcore bosons in one dimension*

$$H = \sum_j \epsilon b_j^\dagger b_j + \sum_{\langle j,k\rangle} t_{j,k} b_j^\dagger b_k \quad (33)$$

where b_i is the bosonic annihilation operator, $t_{j,k}$ is the nearest neighbour hopping.

```
num_sites = 8
hc_bosons_Lattice1d = Lattice1d_hardcorebosons(
    num_sites=num_sites, boundary="periodic", t
    =1)
[Hamiltonian, StatesPerRepr] = bosons_Lattice1d.
    Hamiltonian(filling=2, kval=0)
```

Listing 12. Python example

5. *Spinless fermions in one dimension*

$$H = \sum_j (\epsilon - \mu) c_j^\dagger c_j + \sum_{\langle j,k\rangle} t_{j,k} c_j^\dagger c_k \quad (34)$$

where c_i is the fermionic annihilation operator, $t_{j,k}$ is the nearest neighbour hopping.

```
num_sites = 8
fermions_Lattice1d = Lattice1d_fermions(
    num_sites=num_sites, boundary="periodic", t
    =1)
[Hamiltonian, StatesPerRepr] =
    fermions_Lattice1d.Hamiltonian(filling=2,
    kval=0)
```

Listing 13. Python example

6. *Basis symmetrization of Fermi-Hubbard model*

An instance of the Lattice1d_fermi_Hubbard() may be defined.

```
num_sites = 4
fermiHubbardLattice1d = Lattice1d_fermi_Hubbard(
    num_sites=num_sites, boundary="periodic", t
    =1, U=1, V=2)
[Hamiltonian, basisReprUp, DownStatesPerRepr,
    normHubbardStates] = fermiHubbardLattice1d.
    Hamiltonian(fillingUp=2, fillingDown=2, kval
    =0)
```

Listing 14. Python example

```
In[1]:basisReprUp
Out[1]:array([[0., 0., 1., 1.],
       [0., 1., 0., 1.]])
```

Listing 15. Python example

```
In[2]:DownStatesPerRepr
Out[2]:{0: array([[0., 0., 1., 1.],
        [0., 1., 0., 1.],
        [0., 1., 1., 0.],
        [1., 0., 0., 1.],
        [1., 0., 1., 0.],
        [1., 1., 0., 0.]]),
 1: array([[0., 0., 1., 1.],
        [0., 1., 0., 1.],
        [0., 1., 1., 0.],
        [1., 0., 1., 0.]])}
```

Listing 16. Python example

If we had obtained the Hamiltonian in the $|N\rangle$ basis,

```
[Hamiltonian_N, basisStatesUp, basisStatesDown,
    normHubbardStates] = fermiHubbardLattice.
    Hamiltonian(fillingUp=2, fillingDown=2)
```

Listing 17. Python example

```
In[4]:basisStatesUp
Out[4]:array([[0., 0., 1., 1.],
       [0., 1., 0., 1.],
       [0., 1., 1., 0.],
       [1., 0., 0., 1.],
       [1., 0., 1., 0.],
       [1., 1., 0., 0.]])
```

Listing 18. Python example

```
In[5]:basisStatesDown
Out[5]:array([[0., 0., 1., 1.],
       [0., 1., 0., 1.],
       [0., 1., 1., 0.],
       [1., 0., 0., 1.],
       [1., 0., 1., 0.],
       [1., 1., 0., 0.]])
```

Listing 19. Python example

basisStatesUp and basisStatesDown gives the basis vectors in the cycle/ equivalence set with the specified number of excitations i.e. filling.

In basisReprUp of the $|N,k\rangle$ basis we have only a subset of the basis vectors in basisStatesUp of $|N\rangle$ basis. qutip-lattice chooses as the lowest binary value basis vector to be the representative of the vectors that are translationally related. The two vectors represented by the $[0.,0.,1.,1.]$ and $[0.,1.,0.,1.]$ are the two representative vectors of the two equivalence classes.

The basis in the $|N,k\rangle$ basis is formed by a representative from basisReprUp and one basis state from DownStatesPerRepr's corresponding entry. For example $[0.,1.,0.,1.]$ from basisReprUp and $[0.,1.,1.,0.]$ from corresponding DownStatesPerRepr[1] denotes the following state in the $|N=2,k\rangle=0$ basis, (The positional indices are labelled 0 through 3.)

$$|\bar{n},k\rangle = \frac{\sqrt{p(\bar{n})}}{L}\sum_{l=0}^{L-1}\omega_k^{-l}\hat{T}^l c^\dagger_{1,\uparrow}c^\dagger_{3,\uparrow}c^\dagger_{1,\downarrow}c^\dagger_{2,\downarrow}|vac\rangle \quad (35)$$

The equivalent equation of eq. 20 now factores in the fermion anticommutation sign contributions as well.

$$\sum_{l=1}^{N} phase factor accrued in translation by 1 \neq 0 \quad (36)$$

Only entries compatible with eq. 36 are taken in the construction of DownStatesPerRepr.

VII. DEFINING OBSERVABLES

Symmetrized bases can reduce the computational burden, but finding the operators in them is not quite as straightforward. For, example calculation of the Hamiltonian in the symmetrized basis proceeds in three steps [9]. If $\{|r\rangle\}$ is the set of representative basis vectors, 1) Finding configuration $|n\rangle$ and corresponding amplitude h, so that $H|r\rangle = h|n\rangle$, 2) identifying a symmetry transformation g_n that maps $|n\rangle$ to its representative $|r'\rangle$. 3) Calculating

$$\langle r'|H|r\rangle = \sqrt{\frac{N(r',k)}{N(r,k)}}\chi^k(g_n)h \quad (37)$$

qutip-lattice calculates the Hamiltonian for the user and provides the unitary matrices that relates the two basis. This unitary matrix can help form any operator in the new basis, if it is known in one basis with reasonable effort. For example,

```
[Hamiltonian, basisStatesUp, basisStatesDown,
    normHubbardStates] = fermiHubbardLattice.
    Hamiltonian( fillingUp=None, fillingDown=
    None, kval=None)
```

Listing 20. Hamiltonian written in the full basis

In order to calculate the ground state expectation values of the particle densities we find the ground state first.

```
ES = Hamiltonian.eigenstates(sparse=True, sort='
    low', eigvals=20, tol=0, maxiter=100000)
GS = Qobj(ES[1][0])
Mds = GS.dag() * GS
mods = np.sqrt( Mds[0,0])
GS = GS / mods
```

Listing 21. Finding the ground state

In the full basis, the density operator at site i, n_i is easy to calculate and the function n_i provides that functionality.

```
niu = np.zeros((nSites), dtype=complex)
nid = np.zeros((nSites), dtype=complex)
for i in range(nSites):
    ni_op = n_i(i, basisStatesUp,
    basisStatesDown)
    riu = GS.dag() * ni_op[0] * GS
    niu[i] = riu[0][0]
    rid = GS.dag() * ni_op[1] * GS
    nid[i] = rid[0][0]
```

Listing 22. Calculating densities in the full basis

The density may be plotted.

```
x = np.arange(nSites)
plt.rcParams["figure.figsize"] = [6, 3.50]
plt.rcParams["figure.autolayout"] = True
markerline, stemlines, baseline = plt.stem(x, np
    .real(niu), linefmt='grey', markerfmt='*',
    bottom=0)
markerline, stemlines, baseline = plt.stem(x, np
    .imag(niu), linefmt='grey', markerfmt='*',
    bottom=0)
markerline.set_markerfacecolor('red')
plt.show()
```

Listing 23. plotting the groundstate expectation value of the electron densities

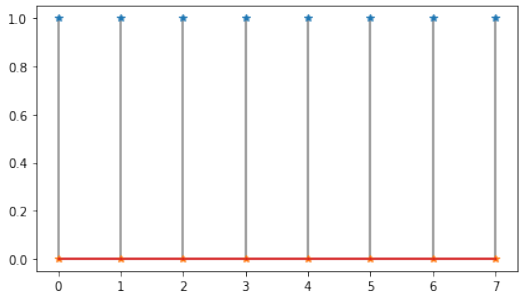

FIG. 4. Spin up electron expectation values in the ground state.

The unitary transformations that achieve the block diagonalization in the

```
Usss = fermiHubbardLattice1d.NoSym_DiagTrans()
Hamiltonian_ki = Usss * Hamiltonian_ * Usss.dag
    ()
Hamiltonian_ki = Hamiltonian_ki.full()
nB = np.shape(Hamiltonian_ki)[0]
for i in range(nB):
    for j in range(nB):
        if np.abs(Hamiltonian_ki[i,j]) < 1e-8:
            Hamiltonian_ki[i, j] = 0
plt.spy(np.abs(Hamiltonian_ki))
plt.show()
```

Listing 24. Python example

The block diagonal from of the Hamiltonian would be plotted.

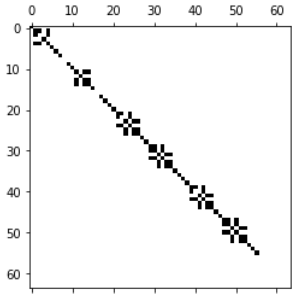

FIG. 5. Bloch diagonal Hamiltonian in the $|k\rangle$ basis.

The Hamiltonian for a specific k-block can be found with the code.

```
Usss_k0 = fermiHubbardLattice1d.
    NoSym_DiagTrans_k(0)
Ham_k0 = Qobj(Usss_k0) * Hamiltonian_ * Qobj(
    Usss_k0).dag()
H_k0 = Ham_k0.full()
```

Listing 25. Python example

Or simply directly, we ask for the Hamiltonian in the $|k\rangle$ basis.

```
[H_k0, basisReprUp, DownStatesPerRepr,
    normHubbardStates] = fermiHubbardLattice1d.
    Hamiltonian( fillingUp=None, fillingDown=
    None, kval=0)
```

Listing 26. Python example

Now, finding the electron density operator (or any other operator) in the $|k\rangle$ basis is not easy as mentioned before. If any operator is known in the full basis the unitary transformation can be used to find it in the $|k\rangle$ basis as well.

```
n_ik = Usss_k0 * n_i(i, basisStatesUp,
    basisStatesDown) * Usss_k0.dag()
```

Listing 27. operator in the $|k\rangle$ basis

We can go in the opposite direction as well, if the operator is known in one basis, the unitary transformations can help find them in the other.

VIII. TOPOLOGICAL INVARIANTS

For most general treatise, see ref. [17]. Response coefficients like charge polarization P_1, Hall conductance σ_{xy}, the quantization of magneto-electric polarizability P_3 can be aptly put as quantized topological invariants in terms of the Berry phase vector potential $\mathcal{A}$,

$$P_1 = -\frac{e}{2\pi}\int_{1dBZ} Tr[\mathcal{A}] \quad (38)$$

$$\sigma_{xy} = -\frac{e^2}{2\pi h}\int_{2dBZ} Tr[d\mathcal{A} + i\mathcal{A}\wedge\mathcal{A}] \quad (39)$$

$$P_3 = -\frac{e^2}{4\pi h}\int_{3dBZ} Tr[\mathcal{A}\wedge d\mathcal{A} + \frac{2i}{3}\mathcal{A}\wedge\mathcal{A}\wedge\mathcal{A}] \quad (40)$$

$\mathcal{A}$ has components $[\mathcal{A}_i(\mathbf{k})]^{\mathbf{mn}} = -\mathbf{i}\langle\mathbf{u_k^m}|\partial_{\mathbf{k_i}}|\mathbf{u_k^n}\rangle$, and $|u_{\mathbf{k}}^n\rangle$ is the Bloch function of band n.

A generalization of P_1 to higher multipole moments was given in ref [17]. These higher moments are of topological origin and depends on the symmetries of the crystal. The primitive dipole, quadrupole, and octupole moments of a continuum quantity, volume charge for example, are defined as

$$p_i = \int d^3\mathbf{r}\rho(\mathbf{r})\mathbf{r_i},$$
$$q_{ij} = \int d^3\mathbf{r}\rho(\mathbf{r})\mathbf{r_i}\mathbf{r_j}, \quad \mathbf{o_{ijk}} = \int \mathbf{d^3}\mathbf{r}\rho(\mathbf{r})\mathbf{r_i}\mathbf{r_j}\mathbf{r_k}. \quad (41)$$

p_i is a Berry phase of the bulk electron states manifesting itself through the surface charge. Analogously, 2d(3d) with square(cubic) shape has edge(corner) charge density quantities calculable from the quadrupole moment q_{xy},

$$p_j^{edge\alpha} = n_i^\alpha q_{ij}, \quad Q^{corner\ \alpha,\beta} = n_i^\alpha n_j^\beta q_{ij} \quad (42)$$

In the hierarchy, octupole moments produce,

$$q_{ij}^{face\ \alpha} = n_i^\alpha o_{ijk}, \quad p^{hinge\ \alpha,\beta} = n_i^\alpha n_j^\beta o_{ijk}$$
$$Q^{corner\ \alpha,\beta,\gamma} = n_i^\alpha n_j^\beta n_k^\gamma o_{ijk} \quad (43)$$

Here $p_j^{edge\alpha}(p^{hinge\ \alpha,\beta})$ are the edge (hinge) tangential polarization per unit length on the square(cube), $q_{ij}^{face\ \alpha}$ are the surface quadrupoles per unit area of the cube, $Q^{corner\ \alpha,\beta,\gamma}$ are the localized corner charges. $n_i^\alpha = s_\alpha\delta_i^{|\alpha|}$ (with $s_{\alpha=\pm} = \pm 1$) is the outward pointing unit normal. Edge polarizations and corner charges are both boundary manifestations of the bulk. The quadrupole and octupole moments are quantized due to reflection symmetries.

1. *Example of quantized quadruple moment:*

A 2d crystal should have i) at least two occupied bands, ii) symmetries quantizing bulk quadrupole and dipole moment for it to have quantized quadrupole moments.

$$h^q(\mathbf{k},\delta) = (\gamma + \lambda\cos(\mathbf{k_x}))\mathbf{\Gamma_4} + \lambda\sin(\mathbf{k_x})\mathbf{\Gamma_3} + (\gamma + \lambda\cos(k_y))\Gamma_2 + \lambda\sin(k_y)\Gamma_1 + \delta\Gamma_0 \quad (44)$$

$\Gamma_0 = \tau_3\sigma_0$, $\Gamma_k = -\tau_2\sigma_k$, $\Gamma_4 = \tau_1\sigma_0$ for $k = 1,2,3$; τ,σ are Pauli matrices for the degrees of freedom in the unit cell. Diagonalizing,

$$E = \pm\sqrt{2\lambda^2 + 2\gamma^2 + 2\lambda\gamma(\cos(k_x) + \cos(k_y))}, \quad (45)$$

each band is two-fold degenrate and gapped unless $\gamma/\lambda = \pm 1$.

With $\hat{m}_x = \tau_1\sigma_3, \hat{m}_y = \tau_1\sigma_1$ and reflection symmetries: $M_x : x \to -x$, and $M_y : y \to -y$, $h^q(\delta = 0)$ has the following reflection symmetries:

$$\hat{m}_x h^q(\mathbf{k}, \delta = \mathbf{0})\hat{\mathbf{m}}_\mathbf{x}^\dagger = \mathbf{h^q(M_x k)}$$
$$\hat{m}_y h^q(\mathbf{k}, \delta = \mathbf{0})\hat{\mathbf{m}}_\mathbf{y}^\dagger = \mathbf{h^q(M_y k)}$$

Additionally, $M_x(k_x, k_y) = (-k_x, k_y)$, $M_y(k_x, k_y) = (k_x, -k_y)$. These symmetries quantize polarizations p_x, p_y and q_{xy}. Also, the model preservis Charge Conjugation(CC, $\hat{C} = \Gamma_0 K$) symmetry, Time Reversal (TR,$\Theta = K$) symmetry, and C_4 symmetry [17].

2. Nested Wilson Loops

When the bulk ends in a boundary cut along x or y direction, the bulk topological moment q_{xy} generates a topologically protected edge. We define the Wilson loop operators in the x and y directions, $\mathcal{W}_{x,\mathbf{k}}$ and $\mathcal{W}_{y,\mathbf{k}}$ respectively. In a crystal with N_{orb} degrees of freedom per unit cell and N_{occ} occupied energy bands, has the occupied Bloch functions, $|u^n_\mathbf{k}\rangle$, for n=1,2,..., N_{occ}, with components $[u^n_\mathbf{k}]$ for $\alpha = 1, 2, ..., N_{orb}$. We also define, $[F_{x,\mathbf{k}}]^{mn} = \langle u^m_{\mathbf{k}+\mathbf{\Delta k_x}}|u^n_\mathbf{k}\rangle$, with $\mathbf{\Delta k_x} = (\mathbf{2\pi/N_x, 0})$.

$$\mathcal{W}_{x,\mathbf{k}} = F_{x,\mathbf{k}+\mathbf{N_x\Delta k_x}}....F_{x,\mathbf{k}+\mathbf{\Delta k_x}}F_{x,\mathbf{k}} \quad (46)$$

A Wannier Hamiltonian of the x-edge can be defined

$$\mathcal{W}_{x,\mathbf{k}} \equiv e^{iH_{\mathcal{W}_x(\mathbf{k})}} \quad (47)$$

$H_{\mathcal{W}_x}(\mathbf{k})$ has eigenvalues $2\pi\nu^j_x(k_y)$, $j = 1, 2, ..., N_{occ}$ which is a function of coordinate k_y of the Wilson loop base point $\mathbf{k}$, (vice versa for y coordinate quantities). With full periodic boundary conditions, the Wilson loop diagonalizes as,

$$\mathcal{W}_{x,\mathbf{k}} = \sum_{j=\pm} e^{2\pi i\nu^j_x(k_y)}|\nu^j_{x,\mathbf{k}}\rangle\langle\nu^j_{x,\mathbf{k}}|, \quad (48)$$

with j=1,2.

When the system is gapped, the Wannier bands can carry their own topological invariants which can be calculated via the nested Wilson loops. A definition of Wannier band subspace would come in handy,

$$|w^\pm_{x,\mathbf{k}}\rangle = \sum_{n=1,2}|u^n_\mathbf{k}\rangle[\nu^\pm_{x,\mathbf{k}}]^m \quad (49)$$

We also define $F^\pm_{y,\mathbf{k}} = \langle w^\pm_{x,\mathbf{k}+\mathbf{\Delta k_y}}|w^\pm_{x,\mathbf{k}}\rangle$, where $\Delta k_y = (0, 2\pi/N_y)$. The nested Wilson loops along k_y in the Wannier bands $\nu^\pm_x$ are

$$\tilde{\mathcal{W}}^\pm_{y,k_x} = F^\pm_{y,\mathbf{k}+\mathbf{N_y\Delta k_y}}.....F^\pm_{y,\mathbf{k}+\mathbf{\Delta k_y}}F^\pm_{y,\mathbf{k}} \quad (50)$$

with their associated polarizations,

$$p_y^{\nu^\pm_x} = -\frac{i}{2\pi N_x}\sum_{k_x} Log\left[\tilde{\mathcal{W}}^\pm_{y,k_x}\right] = \begin{cases} 0, |\gamma|/|\lambda| > 1 \\ 1/2, |\gamma|/|\lambda| < 1 \end{cases} \quad (51)$$

The subspace of occupied energy bands has trivial polarization along y, and each of the separate Wannier band subspaces has non-vanishing polarization. In the thermodynamic limit, the polarization of the Wannier band,

$$p_y^{\nu^\pm_x} = -\frac{1}{(2\pi)^2}\int_{BZ}\tilde{A}^\pm_{y,\mathbf{k}}d^2\mathbf{k}, \quad (52)$$

with the Berry potential over the Wannier band $\nu^\pm_x$ respectively,

$$\tilde{A}^\pm_{y,\mathbf{k}} = -i\langle w^\pm_{x,\mathbf{k}}|\partial_{k_y}|w^\pm_{x,\mathbf{k}}\rangle \quad (53)$$

The reflection symmetry preservation quantize the quadruple moment. Under reflections $x \to -x(M_x)$, $y \to -y(M_y)$, and inversion $(x, y) \to (-x, -y)$, the polarization of the Wannier band subspace obeys,

$$p_y^{\nu^+_x} \overset{\mathrm{M}_x}{=} p_y^{\nu^-_x},\ p_y^{\nu^\pm_x} \overset{\mathrm{M}_y}{=} -p_y^{\nu^\pm_x},\ p_y^{\nu^+_x} \overset{\mathrm{I}}{=} -p_y^{\nu^-_x} mod 1 \quad (54)$$

The Wannier sector polarizations $p_y^{\nu^\pm_x}$ and $p_x^{\nu^\pm_y}$ take the quantized values,

$$p_y^{\nu^\pm_x}, p_x^{\nu^\pm_y} \overset{\mathrm{I,M}_x,\mathrm{M}_y}{=} 0 \text{ or} 1/2 \quad (55)$$

A. Chern number

In 2D, the transverse current in response to a longitudinal electric field $\mathbf{E}$ in the linear response regime is proportional to the topological invariants of the energy bands [18]. This transverse current is quantized and with the Fermi energy ϵ_F in the energy gap, the transverse current is quantized and is proportional to the total Chern number $C_1(\epsilon_F)$ of the occupied bands [19].

$$j_l = \frac{e^2}{h}C_1(\epsilon_F)\epsilon_{lm}E_m,$$
$$C_1(\epsilon_F) = \sum_{\epsilon_\alpha < \epsilon_F}\frac{1}{2\pi i}\int_{BZ}F^\alpha_{xy}(\mathbf{k})\mathbf{d^2k}, \quad (56)$$

with $F^\alpha_{xy}(\mathbf{k}) = \partial_{\mathbf{k_x}}\mathbf{A^\alpha_y}(\mathbf{k}) - \partial_{\mathbf{k_y}}\mathbf{A^\alpha_x}(\mathbf{k})$ being the Berry curvature and $A^\alpha_l(\mathbf{k}) = \langle\psi^\alpha(\mathbf{k})|\partial_\mathbf{l}|\psi^\alpha(\mathbf{k})\rangle$ the Berry connection.

For degenerate energy bands, the formula generalizes to[20],

$$C_1(\epsilon_F) = \frac{1}{2\pi i}\int_{BZ}Tr\left[F_{xy}(\mathbf{k})\right]d^2k$$

with the non-Abelian Berry curvature, $\left(F^{\alpha}_{xy}(\mathbf{k})\right)^{\alpha\beta} = \partial_{k_x} A^{\alpha\beta}_{y}(\mathbf{k}) - \partial_{\mathbf{k_y}} \mathbf{A}^{\alpha\beta}_{\mathbf{x}}(\mathbf{k}) + \mathbf{i}\left[\mathbf{A_x}, \mathbf{A_y}\right]^{\alpha\beta}$, and $\left(A_{\mu}(\mathbf{k})\right)^{\alpha\beta} = \langle\psi^{\alpha}(\mathbf{k})|\nabla|\psi^{\beta}(\mathbf{k})\rangle$ the Berry connection.

B. Winding numbers

The non-Hermitian point-gap topology for a single energy band in a 1D system is characterized by the winding number [21]:

$$W := \int_{-\frac{\pi}{a}}^{\frac{\pi}{a}} \frac{dk}{2\pi i} \frac{d}{dk} ln\left[\omega(k) - \omega_0\right], \tag{57}$$

ω is a normalized complex eigenfrequency, $\omega(k)$ is the closed loop traversed in the complex plane as k is sweeped over the 1d first Brillouin Zone ($-\frac{\pi}{a} \leq k < \frac{\pi}{a}$), a being the lattice constant. W enumerates the number of times $\omega(k)$ winds about the reference frequency ω_0 in the complex frequency plane. A counterclock-wise(clockwise) winding is represented by +(-) sign. Multiband generalization of W is also defined [22]. Nontrivial topological winding must necessarily break symmetry in k, $\omega(k) = \omega(-k)$. Since reciprocity is responsible for this symmetry, non-Hermiticity is a requirement for nontrivial topological winding [21].

The concept readily generalizes to 2d. In a 2d square lattice with dispersion $\omega(k_x, k_y)$, circular paths can be found from the periodicity in either k_x or k_y, for example a straight path from $k_x = -\frac{\pi}{a}, k_y$ to $k_x = \frac{\pi}{a}, k_y$ forms a closed loop and we can define a winding number $W(k_y)$.

$$W(k_y) := \int_{-\frac{\pi}{a}}^{\frac{\pi}{a}} \frac{dk}{2\pi i} \frac{d}{dk} ln\left[\omega(k_x, k_y) - \omega_0\right], \tag{58}$$

1. Chiral symmetry and winding: fermionic kitaev chain

$$\hat{H}_F = \sum_k \left[t\cos(k)\hat{c}^{\dagger}_k \hat{c}_k + i\frac{\Delta}{2}\sin(k)\left(\hat{c}^{\dagger}_k \hat{c}^{\dagger}_{-k} - H.c.\right)\right] \tag{59}$$
$$= \frac{1}{2}\sum_k C^{\dagger}_k \left[h_F(k).\hat{\sigma}\right] C_k,$$

with $C^{\dagger}_k = \left(c^{\dagger}_k, c_{-k}\right)$, $h_F(k) = [0, -\Delta\sin(k), t\cos(k)]$, and $\hat{\sigma}$ the vector of Pauli matrices in the particle-hole space. Since $\hat{H}_F(k)$ has chiral symmetry (co-efficient of σ_x is 0 for all k in the first Brillouin Zone), we have the topological winding number defined as the number of times $h_F(k)$ encircles the origin, namely 1 in this model.

2. winding in Bosonic system example

A bosonic model with nonzero winding in momentum space from [23],

$$\hat{H}_B = \sum_k \left[t\sin(k)\hat{a}^{\dagger}_k \hat{a}_k + i\frac{\Delta}{2}\cos(k)\left(\hat{a}^{\dagger}_k \hat{a}^{\dagger}_{-k} - H.c.\right)\right] \tag{60}$$
$$= \frac{1}{2}\sum_k A^{\dagger}_k \left[h_B(k).\hat{\sigma}\right] A_k,$$

with $A^{\dagger}_k = \left(a^{\dagger}_k, a_{-k}\right)$, $h_B(k) = [0, -\Delta\cos(k), t\sin(k)]$ has a winding of 1. In real space,

$$\hat{H}_B = \frac{1}{2}\sum_j \left[it\hat{a}^{\dagger}_{j+1}\hat{a}_j + i\Delta\hat{a}^{\dagger}_{j+1}\hat{a}^{\dagger}_j + H.c.\right] \tag{61}$$

Since, bosonic operators also have the representation in terms of position and momentum quadrature, $\hat{a}_j = (\hat{x}_j + i\hat{p}_j)/\sqrt{2}$,

$$\hat{H}_B = \frac{1}{2}\sum_j \left[-(t-\Delta)\hat{x}_{j+1}\hat{p}_j + (t+\Delta)\hat{p}_{j+1}\hat{x}_j\right]$$

which is two copies of the Hatano-Nelson model for the x and p lattices. Unitary local squeezing operators can render $\hat{H}_B$ in a form with real hopping $\tilde{t} = \sqrt{t^2 - \Delta^2} = t/\cosh(r)$.

$$\hat{U}\hat{x}_j\hat{U}^{\dagger} = e^{r(j-j_0)}\hat{\tilde{x}}_j, \qquad \hat{U}\hat{p}_j\hat{U}^{\dagger} = e^{-r(j-j_0)}\hat{\tilde{p}}_j \tag{62}$$
$$\hat{U}\hat{H}_B\hat{U}^{\dagger} = \frac{1}{2}\sum_j \left(i\tilde{t}\hat{\tilde{a}}^{\dagger}_{j+1}\hat{\tilde{a}}_j + H.c.\right), \tag{63}$$

where $e^{2r} = (t+\Delta)/(t-\Delta)$. Since, eq. 63 is in a tight-binding form, it is easily diagonalizable in the periodic boundary condition case, with real eigenvalues,

$$E_n = \tilde{t}\cos(k_n), \qquad k_n = n\pi/(N+1). \tag{64}$$

The open boundary condition case or chain, can be diagonalized,

$$\hat{H}^{OBC}_B = \sum_n E_n \hat{\beta}^{\dagger}_n \hat{\beta}_n$$
$$\hat{\beta}_n = \sum_{j=1}^{N}\left[u_n(j)\hat{a}_j - v_n(j)\hat{a}^{\dagger}_j\right]$$
$$u_n(j) = \sqrt{\frac{2}{N+1}} i^{-j}\sin(k_n j)\cosh\left[r(j-j_0)\right],$$
$$v_n(j) = \sqrt{\frac{2}{N+1}} i^{-j}\sin(k_n j)\sinh\left[r(j-j_0)\right] \tag{65}$$

C. Non-Hermitian Quantum Walk: Rudner-Levitov model

[24]

D. Knot invariants of 1d NH system

Ref. [25] propounds a theory characterizing the topology of 1d NHHs with separable bands with knots (or links) formed by the eigenenergy strings. A $\mathbb{Z}_2$ knot invariant, the global biorthogonal Berry phase Q, is shown to be equal the permutation parity of the NH bands. Q is calculable as the sum of the Wilson loop eigenphases. Two types of topological phase transitions were found through the Exceptional Points(EP) when switching between distinct knots (accompanied by abrupt changes in biorthogonal Wannier center).

A 1d NHH with separable bands and no symmetry is fully characterized by knots inside a solid torus. The braids of energy eigenvalues are closed since Brillouin Zone is periodic. The complex eigenenergies of a 1d NHH is a set $\mathcal{E} = \{E_j(k)\}$ with band index j=1,2,..,N. In the 3d space spanned by (ReE, ImE, k), the trajectory of $E_i(k)$ is a string as k sweeps through 0 to 2π where the set maps into itself. On a chosed 2d plane parallel to k-axis, the projections of N strings form a sufficient description of the braid. Braid operators codify the interchange of the strings. The complete braid is the product of these operators. Since $\mathcal{E}$ is periodic in k, the braid is a knot. The net result of the evolution of k over one period is the permutation:

$$\sigma = \begin{pmatrix} E_1(0) & E_2(0) & ... & E_N(0) \\ E_1(2\pi) & E_2(2\pi) & ... & E_N(2\pi) \end{pmatrix} \tag{66}$$

The parity $P(\sigma)$ is 1(-1) for even(odd) number of transposition. The $\mathbb{Z}_2$ topological invariant Q is related to P.

The non-Abelian Berry connection $A_B^{mn} = i\langle\partial_i u_{L\alpha}^m(\tilde{\mathbf{k}})|\partial_j u_{R\alpha}^n(\tilde{\mathbf{k}})\rangle$ is defined in terms of left and right eigenvectors. The Berry phase in eq. 113 is called the global biorthogonal Berry phase,

$$Q = \oint_0^{2\pi} dk Tr[A_B] \tag{67}$$

Q turns out to be quantized to 0 and π, for even(odd) band permutations.

$$e^{iQ} = (-1)^{P(\sigma)} \tag{68}$$

The $\mathbb{Z}_2$ knot invariant Q coarsely classifies knots into two groups. Hopf and figure-8 has the same Q namely 0. But finer classification may differnetiate them as well. For NHH, biorthogonal Wilson loops may be defined from the Berry connection,

$$W_B := \mathcal{P} e^{i\oint_0^{2\pi} dk A_B} \tag{69}$$

$$W_B|\mu_n\rangle = e^{i\nu_n}|\mu_n\rangle \tag{70}$$

$\mathcal{P}$ is the path ordering operator. The eigenphases $|\nu_n\rangle$ are called the Wannier centers, and it can be showed that,

$$Q = \sum_n \nu_n \tag{71}$$

Different knots and their phase transitions can be investigated with a twistor: T_n:

$$T_n = \begin{bmatrix} 0 & e^{ink} \\ 1 & 0 \end{bmatrix}, \tag{72}$$

with n counting the number of twists of the two band strings, $E_\pm = \pm e^{ink/2}$, with k evolving from 0 to 2π. The braid word of T_n is simply τ_1^n. The twiston as a NHH for n=0,1,2 gives rise to the unlink, unknot, and Hopf link respectively. Using T_n other Hamiltonians can be formed, for example, with two parameters m_1 and m_2,

$$H_{12}(k) = im_1\sigma_z + m_2 T_1 + T_2 \tag{73}$$

which has three topologically distinct phases (fig. 6(b)). The Hopf link is the blue region, the unlink the green, and the unknot the pink region in the phase diagram in fig. 6(b). The knots are also plotted with the eigenenergy strings as k is sweeped. All three phases show NH skin effect, but line or point gaps cannot distinguish between these knot phases. Eq. 73

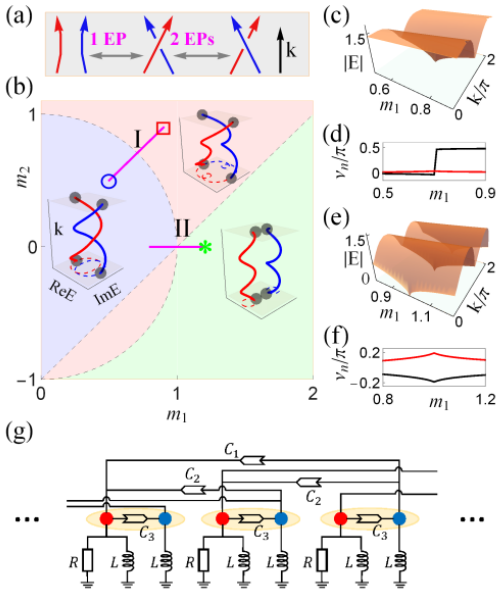

FIG. 6. (a)Schematic phase transitions and (b)Phase diagram for the $H_{12}(k)$ in eq. 73. (c) and (e) plots $|E(m_1, k)|$ along the cut labelled by I and II in (b). An EP is at $(1/\sqrt{2}, \pi)$(c), and two EPs are at (1,0) and $(1, \pi)$ in (e). (d) and (f) show the Wannier centers ν_n along cuts I and II. (g) Schematic of a periodic electric circuit that realizes H_{12}.

IX. NON HERMITIAN LATTICE MODELS

NHH are a partial description, it is necessarily part of a larger system where the probability conserving properties of quantum evolution holds. From NHH, we want to find larger systems with probability conserving physics (not

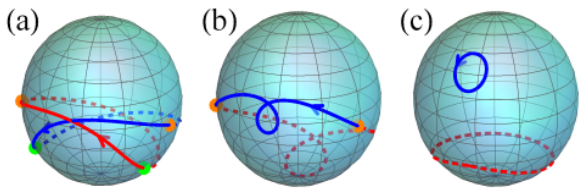

FIG. 7. Characteristic crossing pattern of eigenvectors (points on the bloch sphere) reveal the knot topology, the invariant Q can be read off. The red(blue) curves are the eigenvectors from the north pole, they fall into the solid lines after a long time. (a)$m_1 = m_2 = 0.5$ the Hopf-link phase, (b)$m_1 = m_2 = 0.9$ the unknot phase, and (c)$m_1 = 1.2, m_2 = 0.0$ the unlink phase,

uniquely). When incoherent pump and/or loss is present, the general description eq. by generalizing **??** [3],

$$\frac{\partial}{\partial t}\hat{\rho}(t) = -i\left[\hat{H}(t), \hat{\rho}\right] + \sum_{\mu=1}^{M_{loss}} \mathcal{D}\left[\hat{L}_\mu\right]\hat{\rho}(t) + \sum_{\mu=1}^{M_{gain}} \mathcal{D}\left[\hat{G}_\mu\right]\hat{\rho}(t), \tag{74}$$

$$\hat{L}_\mu = \sum_{j=1}^{N} l_{\mu j}\hat{c}_j, \quad \hat{G}_\mu = \sum_{j=1}^{N} g^*_{\mu j}\hat{c}^\dagger_j \tag{75}$$

The incoherent loss/gain operators are linear in creation/annihilation operators and the Hamiltonian is that of a lattice. $\frac{\gamma_j^D}{2}$ 2Γ The Hamiltonian for a no-jump evolution or post-conditioned evolution (repeating an experiment many times till a run is found with no quantum jumps),

$$\hat{H}_{cond} = \sum_{n,m}\hat{c}^\dagger_n\hat{c}_m - \frac{i}{2}\sum_\gamma L_\gamma \hat{l}^\dagger_\gamma \hat{l}_\mu - \frac{i}{2}\sum_\delta G_\delta\left(1 \mp \hat{g}^\dagger_\delta\hat{g}_\delta\right),$$

- and + are for fermionic and bosonic operators respectively. Also, $\hat{l}_\gamma = \sum_m \langle l_\gamma|m\rangle\hat{c}_m$ and $\hat{g}^\dagger_\delta = \sum_n \langle n|g_\delta\rangle\hat{c}^\dagger_n$. $|\hat{l}_\gamma\rangle$ and $|g_\delta\rangle$ are eigenvectors of the Hermitian positive definite matrices $L_{nm} = \left(\hat{l}^\dagger\hat{l}\right)_{nm}$ and $G_{nm} = \left(\hat{g}^\dagger\hat{g}\right)_{nm}$ respectively. In the evolution of $\hat{\rho}$ dictated by eq. 75, is it possible to find a part of 'drift' dynamics defined by some Hamiltonian?

As done in [3], an evolution equation can be calculated for the normal ordered covariance matrix,

$$i\partial_t\langle\hat{c}^\dagger_n\hat{c}_m\rangle = \sum_a\left(\left(\hat{H}_{eff}\right)_{ma}\langle\hat{c}^\dagger_n\hat{c}_a\rangle - \left(\hat{H}^\dagger_{eff}\right)_{an}\langle\hat{c}^\dagger_a\hat{c}_m\rangle\right) \tag{76}$$

And we observe the dynamics generated by NHH,

$$\hat{H}_{eff} = \hat{H} - \frac{i}{2}\left(\hat{L} \pm \hat{G}\right) \tag{77}$$

For both fermions and bosons, The Hamiltonian $\hat{H}_{eff}$ is similar to $\hat{H}_{cond}$, with signs of the generator operators alternating.

$$\hat{H}_{cond} = \hat{H} - \frac{i}{2}\left(\hat{L} \mp \hat{G}\right) \tag{78}$$

A. Atom-field models

Collective decay/ many body signature [26] [27]

Localized emitters arranged on a lattice are amenable to engineered atom-photon interactions and high fidelity long range interactions between them [26–28]. Qutiplattice package includes code functionality in the single excitation limit. The model was used to investigate atomic emission properties under dipole-dipole interaction coupled interstitial impurities in the array in [28]. With a regular periodic arrangement, translational symmetry aids in the computational challenge as the dynamics problem at each quasi-momentum decouple.

With $|g_i\rangle$ and $|e_i\rangle$ being the emitter/atom's ground and excited states (resonance frequency of ω_0) respectively, the coherent interaction part of the dynamics is encoded in the Hamiltonian,

$$\mathcal{H} = \hbar\sum_{i=1}^{N}\omega_0\hat{\sigma}^i_{ee} + \hbar\sum_{i,j=1}^{N} J^{ij}\hat{\sigma}^i_{eg}\hat{\sigma}^j_{ge} \tag{79}$$

The coherent $J(r_i, r_j)$ and incoherent $\Gamma(r_i, r_j)$ dipole-dipole interaction between two-atoms situated at r_i and r_j,

$$J(r_i, r_j) - \frac{i}{2}\Gamma(r_i, r_j) = -\frac{3\pi\sqrt{\gamma_i\gamma_j}}{\omega_L}\hat{d}^\dagger{}_i.G(r_i, r_j, \omega_L).\hat{d}_j,$$

with the free-space Green's function (the propagator of the electromagnetic field between emitters atr_i and r_j)

$$G_{ij}(r) = \frac{e^{i\omega r}}{4\pi r}\left[\left(1 + \frac{i}{\omega r} - \frac{1}{\omega^2 r^2}\right)\delta_{ij} - \left(1 + \frac{3i}{\omega r} - \frac{3}{\omega^2 r^2}\right)\frac{r_i r_j}{r^2}\right] - \frac{\delta(\mathbf{r})}{3\omega^2}\delta_{ij} \tag{80}$$

$\hat{d}$ is the dipole matrix element of the atomic transition, r=$|\mathbf{r_i} - \mathbf{r_j}|$. The dissipative interactions are codified in the jump operators $\{\hat{O}_\nu\}$, $\nu = 1, 2, .., N$. Each individual jump operator $\{\hat{O}_\nu\}$ is an eigenvector of the $N \times N$ dimensional Γ matrix and the corresponding decay rates are the corresponding eigenvalue Γ_ν. The Γ matrix is composed of the elements Γ_{ij}.

Each jump operator $\hat{O}_\nu$ is a superposition of all the lowering operators,

$$\hat{O}_\nu = \sum_{i=1}^{N}\alpha_{\nu,i}\hat{\sigma}^i_{ge} = \sum_{i=1}^{N}\alpha_{\nu,i}|g_i\rangle\langle e_i| \tag{81}$$

subjectto the normalization,

$$\sum_{i=1}^{N}\alpha^*_{\nu,i}\alpha_{\mu,i} = \delta_{\nu,\mu} \tag{82}$$

The spontaneous emission rate Γ_0 of each atom is found in,

$$\sum_{i=1}^{N} \Gamma_\nu |\alpha_{\nu,i}|^2 = \Gamma_o \tag{83}$$

The total emission rate R is calculated with,

$$R = -\frac{d}{dt}\sum_i \langle \sigma_{ee}^i \rangle = \sum_{i=1}^{N} \Gamma_\nu \langle \hat{O}^\dagger{}_\nu \hat{O}_\nu \rangle \tag{84}$$

In an infinite lattice, excitations are collective surface modes of in-plane quasimomentum $\mathbf{k}$ with lowering operator $\sigma_{\mathbf{k}}$,

$$J(\mathbf{k}) - \frac{\mathbf{i}}{\mathbf{2}}\mathbf{\Gamma}(\mathbf{k}) = -\frac{\mathbf{3}\pi\sqrt{\gamma_\mathbf{i}\gamma_\mathbf{j}}}{\omega_\mathbf{L}} \hat{\mathbf{d}}^\dagger{}_\mathbf{i}.\mathbf{G}(\mathbf{k},\omega_\mathbf{L}).\hat{\mathbf{d}}_\mathbf{j}, \tag{85}$$

$$J(\mathbf{k}) = \sum_\mathbf{i} \mathbf{J}(\mathbf{r_i} - \mathbf{r_s})\mathbf{e}^{-\mathbf{ik}.\mathbf{r_i}}$$

$$\Gamma(\mathbf{k}) = \sum_\mathbf{i} \mathbf{\Gamma}(\mathbf{r_i} - \mathbf{r_s})\mathbf{e}^{-\mathbf{ik}.\mathbf{r_i}},$$

and $G(\mathbf{k},\omega_\mathbf{L})$ is the discrete Fourier Transformation of $G(r_i, r_j, \omega_L)$ over the entire lattice. Interstitial impurities can give rise to new unit cell periodicities and coupled equation structures in the $\mathbf{k}$-space. The interaction picture Hamiltonian with dipole-dipole interaction between emitters and the impurity site is,

$$H_I^{(1)} = \sum_i \left(J(r_i, r_s) - \frac{i}{2}\Gamma(r_i, r_s) \right) \sigma_i^\dagger s + H.c.$$

The effect of geometries was investigated in ref. [29]

B. "No-jump" evolution

Defining the model,

```
nSites = 6
fermiHubbardLattice = Lattice1d_f_Hubbard(
    num_sites=nSites, boundary="periodic", t=1,
    U=-4)
```

Listing 28. Python example

```
[Hamiltonian_Nk, basisReprUp, DownStatesPerRepr,
     normHubbardStates] = fermiHubbardLattice.
    Hamiltonian( fillingUp=4, fillingDown=4,
    kval=0)
```

Listing 29. Python example

C. Scattering matrix of a regular tight binding chain

1. *Photonic/bosonic tight binding chain*

For a cavity mode $\hat{a}_j$ with coherent interaction codified by $\hat{H}_a$ and coupled to a waveguide at a rate κ, the Heisenberg-Langevin equations take the form [30, 31] ,

$$\frac{d}{dt}\hat{a}_j(t) = -i\left[\hat{a}_j(t), \hat{H}_a\right] - \frac{\kappa}{2}\hat{a}_j(t) - \sqrt{\kappa}\hat{a}_{j,in}(t)$$

and the so-called input-output relationship,

$$\hat{a}_{j,out}(t) = \hat{a}_{j,in}(t) + \sqrt{\kappa}\hat{a}_j(t)$$

The retarded Green function of the lattice is defined as

$$G^R(i,j;t) \equiv -i\theta_H(t)\langle\left[\hat{a}_j(t), \hat{a}_j^\dagger(0)\right]\rangle, \tag{86}$$

$\theta_H(t)$ being the Heaviside unit step function. If the cavity was driven by a coherent drive,

$$\langle \hat{a}_{j,in}(t)\rangle = \bar{a}_{in,j}e^{-i\omega t}$$
$$\langle \hat{a}_{j,out}(t)\rangle = \bar{a}_{out,j}e^{-i\omega t}$$
$$\bar{a}_{out,j} = \sum_{j'} s_{jj'}[\omega]\bar{a}_{in,j'}$$
$$s_{jj'}[\omega] = \delta_{jj'} - i\sqrt{\kappa_j\kappa_{j'}}G^R[j,j';\omega] \tag{87}$$

The retarded Green Function in the frequency domain,

$$G_0^R[j,j';\omega] = \left[\frac{1}{(\omega + i\frac{\kappa}{2})\mathbf{1} - \mathbf{H_a}}\right]_{jj'} \equiv \left[\frac{1}{(\omega)\mathbf{1} - \mathbf{H_{eff}}}\right]_{jj'}$$

If a spatially varying loss κ_j is introduced, it effectuates an imaginary potential $\mathbf{V}$ at each site [23].

$$V_{ij} = -i\frac{\kappa_j}{2}\delta_{ij} \tag{88}$$

The full Green function $G^R[\omega]$ is obtained via the Dyson equation,

$$G^R[\omega] = G_0^R[\omega] + G_0^R[\omega]VG^R[\omega] = \frac{1}{\mathbf{1} - \mathbf{G_0^R}[\omega]\mathbf{V}}G_0^R[\omega]$$

The unperturbed Green function for a finite chain of N sites is [23],

$$G_0^R[j,j';\omega]$$
$$= i^{j-j'}\frac{2\sin\{q[\omega]min(j,j')\}\sin\{q[\omega]\,[N+1-max(j,j')]\}}{\tilde{t}\sin\{q[\omega]\}\sin\{q[\omega]\,[N+1]\}},$$

where $q[\omega]$ is the complex wave vector computed from solving,

$$\omega + i\frac{\kappa}{2} - \tilde{t}\cos(q[\omega]) \tag{89}$$

D. Fermionic tight binding chain

For N fermionic sites each coupled to a reservoirs(bath) of fermions, (c_σ, $c_\sigma^\dagger$ being the fermionic annihilation and creation operators respectively, operators under ˜ are the bath operators who are labelled with wavevectors). The coherent parts of the interactions between the fermionic system sites included in H_S, and the coupling to the baths described by,

$$H_{Tot} = H_0 + H_S + H_{int}$$
$$H_0 = \sum_i \epsilon_i c_i^\dagger c_i + \sum_{k_j} \epsilon_{k_j} \tilde{c}_{k_j}^\dagger \tilde{c}_{k_j}$$
$$H_{int} = \left(\sum_{i=1}^{N} V_i \sum_{k_j} c_i^\dagger \tilde{c}_{k_j} + H.c. \right) \quad (90)$$

The density matrix of the system+bath, $\rho(t)$ follows the von Neumann equation,

$$\dot{\rho} = -i[H_{Tot}, \rho(t)] \quad (91)$$

Going into the interaction picture (all interaction picture terms are written with a $\hat{}$), the interaction picture density operator, $\hat{\rho}(t) = e^{iH_0 t}\rho(t)e^{-iH_0 t}$ [32],

$$\dot{\hat{\rho}}(t) = \mathcal{L}(t)\hat{\rho}_0 + \int_0^t dt_1 \mathcal{L}(t)\mathcal{L}(t_1)\hat{\rho}(t_1)$$
$$\mathcal{L}(t)\hat{\rho}(t_1) = -i[\hat{V}(t), \hat{\rho}(t_1)]$$

The L reservoir has the injecting band of particles and R reservoir the transmotted bands. Using the Born approximation, $\hat{\rho}(t) = \hat{\rho}_S(t) \otimes \hat{\rho}_L \otimes \hat{\rho}_R$, we find for the system density operator, $\hat{\rho}_S(t)$, ($\hat{\rho}_{L(R)}$ is the density operator of the L(R) reservoir)

$$\dot{\hat{\rho}}_S(t) = -i \int_0^t dt_1 \sum_{i,j} \Big[g_{ij}^{>}(t,t_1)\hat{d}_i^\dagger(t)\hat{d}_j(t_1)\hat{\rho}_S(t_1)$$
$$-g_{ji}^{>}(t_1,t)\hat{d}_i(t)\hat{\rho}_S(t_1)\hat{d}_j^\dagger(t_1) - g_{ji}^{<}(t_1,t)\hat{d}_i(t)\hat{d}_j^\dagger(t_1)\hat{\rho}_S(t_1)$$
$$+g_{ij}^{<}(t,t_1)\hat{d}_i^\dagger(t)\hat{\rho}_S(t_1)\hat{d}_j(t_1)\Big] + H.c. \quad (92)$$

The first order correlation functions appearing in eq. 92 have the following definitions,

$$g_{ij}^{<}(t,t') = \delta_{ij}|V_i|^2 \sum_{k_i} i\langle \hat{c}_{k_i}^\dagger(t')\hat{c}_{k_i}(t)\rangle$$
$$g_{ij}^{>}(t,t') = \delta_{ij}|V_i|^2 \sum_{k_i} (-i)\langle \hat{c}_{k_i}(t)\hat{c}_{k_i}^\dagger(t')\rangle$$

They can be approximated by the so-called wideband approximation.

$$g_{ij}^{<}(t,t') = i\delta_{ij}2\pi\mathcal{D}_i|V_i|^2 f_i \delta(t-t')$$
$$g_{ij}^{>}(t,t') = -i\delta_{ij}2\pi\mathcal{D}_i|V_i|^2(1-f_i)\delta(t-t')$$

Here f_i is the Fermi function and $\mathcal{D}_i$ is a constant density of states in the i-th reservoir. Fermi functions take the values $f_i = 0 (f_i = 1)$ for the drain (source) reservoir. With $\Gamma_i = 2\pi\mathcal{D}_i|V_i|^2$ being the strength of the coupling to the reservoir, we can use the wideband approximations to derive the Schrödinger picture Lindblad equation [32],

$$\dot{\rho}_S = -i[H_S, \rho_S] - \frac{1}{2}\sum_i \Gamma_i \left[f_i \mathcal{L}_i^+ \rho_S + (1-f_i)\mathcal{L}_i^- \rho_S \right], \quad (93)$$

with $\mathcal{L}_i^+\rho_S = c_i c_i^\dagger \rho_S + \rho_S c_i c_i^\dagger - 2c_i^\dagger \rho_S c_i$, and $\mathcal{L}_i^-\rho_S = c_i^\dagger c_i \rho_S + \rho_S c_i^\dagger c_i - 2c_i \rho_S c_i^\dagger$ codify the dissipative action of the reservoir to site i.

The integro-differential equation in 92 simplies to a differential equation 93 with the wide-band approximation.

The vectorized system density matrix, $\vec{\rho}_S = \mathbf{vec}[\rho_\mathbf{S}]$, follow a numerically amenable diffierential equation [33].

$$\vec{\rho}_S(t) = e^{-i\mathcal{M}t}\vec{\rho}_S(0) \quad (94)$$

The $\mathcal{M}$ matrix has the structure [32],

$$\mathcal{M} = \mathcal{M}_0 - i\frac{\Gamma}{2}$$
$$\mathcal{M}_0 = I^{\otimes 3} \otimes H_S - H_S^T \otimes I^{\otimes 3}$$

I being the 2d identity matrix. The structure of $\mathcal{M}$ holds the signatures of NHH that is induced by the coupling to the reservoirs. A passing note on the numerics is that before integrating eq. 94, the fermionic operators have to be replaced by spin operators with the Jordan Wigner transformation.

X. CORRELATED RADIANCE IN EMITTERS COUPLED TO NONLINEAR PHOTONIC CAVITY

Translational symmetry techniques can be availed of in computing dynamics problems involving nonlinear cavities which are always very demanding [34]. Two or multiple photon bound states can be used in ansatzes that carry the essential support of the wavefunction in certain dynamics problems[35, 36].

H_B in eq. 31 with energy ω_c and tunneling amplitude J,

$$H_{ph} = \sum_n \omega_c a_n^\dagger a_n - \frac{U}{2}a_n^\dagger a_n^\dagger a_n a_n - J\left(a_n^\dagger a_{n+1} + H.c.\right)$$

N two Level System(TLS) are each coupled to a cavity of the one dimensional lattice.

$$H = H_{ph} + \frac{\omega_e}{2}\sum_{i=1}^{N}\sigma_i^z + g\sum_{i=1}^{N}\left(a_{n_i}\sigma_i^+ + a_{n_i}^\dagger\sigma_i^-\right) \quad (95)$$

For N=2, the essential physics is found in a subspace of wave-functions with two-photon bound states[35, 36].

$$|\phi_2\rangle(t) = e^{-2i\omega_e t}\Bigg\{ c_e(t)\sigma_1^+\sigma_2^+ + \sum_K c_K(t)B_K^\dagger$$
$$+\sum_k \left[c_{1k}(t)\sigma_1^+ + c_{2k}(t)\sigma_2^+\right]a_k^\dagger \Bigg\}|g,g,vac\rangle, \quad (96)$$

with $a_k^\dagger = \sum_n e^{ikn} a_n^\dagger/\sqrt{N_c}$ and $B_K^\dagger$ is creation operator of a boundstate of two photons, $|\Psi_K^b\rangle = B_K^\dagger|vac\rangle$.

Writing the photon number conserving bose Hubbard model in the k-space, all the different k-s decouple. the cross terms of the Hamiltonian are zero because it is particle number conserving. The first term with no explicit k-dependence can have diagonal in k- resolution as well,

$$\mathbf{1} \equiv \sum_{\mathbf{k}} |\mathbf{k}\rangle\langle\mathbf{k}| \tag{97}$$

Therefore it is possible to solve the individual k-value dynamics separately as the interactions are decoupled in k.

XI. NON HERMITIAN SYMMETRIES

For a review, see [37] and a recent one for $\mathcal{PT}$-symmetry in photonic systems, see [38, 39].

A. $\mathcal{PT}-$ *symmetry*

Any Hamiltonian $\hat{H}_{NH}$ is parity-time reversal ($\hat{\mathcal{P}}\hat{\mathcal{T}}$) symmetric if there exists a unitary operator $\hat{\mathcal{P}}$ and an antiunitary operator $\hat{\mathcal{T}}$ such that

$$\left[\hat{\mathcal{P}}\hat{\mathcal{T}}, \hat{H}_{NH}\right] = 0 \tag{98}$$

$$(\hat{\mathcal{P}}\hat{\mathcal{T}})^2 = \mathbb{1} \tag{99}$$

Eq. 98 dictates that if $|\psi\rangle$ is a right eigenstate of $\hat{H}_{NH}$ with eigenvalue E, then $\hat{\mathcal{P}}\hat{\mathcal{T}}|\psi\rangle$ is a right eigenstate with eigenvalue E^*. As such the first possibility is that $|\psi\rangle \propto \hat{\mathcal{P}}\hat{\mathcal{T}}|\psi\rangle$, and $|\psi\rangle$ is an eigenstate of $\hat{\mathcal{P}}\hat{\mathcal{T}}$ and E is real, hence $\hat{\mathcal{P}}\hat{\mathcal{T}}$-symmetry is unbroken. The other distict possibility is that $|\psi\rangle$ and $\hat{\mathcal{P}}\hat{\mathcal{T}}|\psi\rangle$ are distinct eigenstates with eigenvalue E_n and E_n^* and $\hat{\mathcal{P}}\hat{\mathcal{T}}$-symmetry is broken.

The representations of $\hat{\mathcal{P}}$ and $\hat{\mathcal{T}}$ depends on the system under study. In most cases, $\hat{\mathcal{T}}$ is the complex conjugation operator and $\hat{\mathcal{P}}$ or $\hat{\mathcal{T}}$ do not necessarily have to codify parity or time-reversal resepectively. For the following,

$$\hat{H}_{NH} = \begin{bmatrix} m+\Delta & ite^{i\theta} \\ it'e^{-i\theta} & m-\Delta \end{bmatrix}, \quad m, \Delta, t, t' \in \mathbb{R},\ t \neq -t'$$

the following unitary operator $\hat{C}$,

$$\hat{H}_{NH} = \begin{bmatrix} e^{i\theta} & 0 \\ 0 & -e^{-i\theta} \end{bmatrix}, \quad \theta \neq n\pi,\ n \in \mathbb{N}$$

can be found which does not satisfy $(\hat{C})^2 = \mathbb{1}$, but satisfy $(\hat{C}\hat{\mathcal{T}})^2 = \mathbb{1}$, $\hat{\mathcal{T}}$ being the complex conjugation. Now, $\left[\hat{C}\hat{\mathcal{T}}, \hat{H}_{NH}\right] = 0$ and eigenvalues of $\hat{H}_{NH}$ is coincident real or complex conjugate pair.

Eq. 99 can also be generalized to some c-number times identity operator on the right hand side, for example -1 which gives the interesting result of $|\psi\rangle$ and $\hat{\mathcal{P}}\hat{\mathcal{T}}|\psi\rangle$ being orthogonal.

B. Anti-$\mathcal{PT}-$ *symmetry*

Any Hamiltonian $\hat{H}_{NH}$ is anti-parity-time reversal (anti-$\hat{\mathcal{P}}\hat{\mathcal{T}}$) symmetric if there exists a unitary operator $\hat{\mathcal{P}}$ and an antiunitary operator $\hat{\mathcal{T}}$ such that

$$\left\{\hat{\mathcal{P}}\hat{\mathcal{T}}, \hat{H}_{NH}\right\} = 0 \tag{100}$$

$$(\hat{\mathcal{P}}\hat{\mathcal{T}})^2 = \mathbb{1} \tag{101}$$

Eq. 100 dictates that if $|\psi\rangle$ is a right eigenstate of $\hat{H}_{NH}$ with eigenvalue E, then $\hat{\mathcal{P}}\hat{\mathcal{T}}|\psi\rangle$ is a right eigenstate with eigenvalue $-E^*$. As such the first possibility is that $|\psi\rangle \propto \hat{\mathcal{P}}\hat{\mathcal{T}}|\psi\rangle$, and $|\psi\rangle$ is an eigenstate of $\hat{\mathcal{P}}\hat{\mathcal{T}}$ and E is imaginary, hence $\hat{\mathcal{P}}\hat{\mathcal{T}}$-anti-symmetry is unbroken. The other distict possibility is that $|\psi\rangle$ and $\hat{\mathcal{P}}\hat{\mathcal{T}}|\psi\rangle$ are distinct eigenstates with eigenvalue E_n and $-E_n^*$ and $\hat{\mathcal{P}}\hat{\mathcal{T}}$-antisymmetry is broken.

Anti-$\mathcal{PT}-$ *symmetry* and $\mathcal{PT}-$ *symmetry* can be combined into a more general form, ($\phi \in [0, 2\pi)$)

$$\hat{\mathcal{P}}\hat{\mathcal{T}}\hat{H}_{NH} = e^{i\phi}\hat{H}_{NH}\hat{\mathcal{P}}\hat{\mathcal{T}} \tag{102}$$

C. Pseudo-Hermiticity

Pseudo-Hermiticity is a envelope generalization of Hermiticity and $\hat{\mathcal{P}}\hat{\mathcal{T}}$ symmetry and can indicate the ability of a NHH to possess real eigenvalues. For a NHH, $\hat{H}_{NH}$ the condition

$$\eta\hat{H}_{NH}\eta^{-1} = \hat{H}_{NH}^\dagger, \tag{103}$$

with some invertible Hermitian linear operator η indicate pseudo-hermiticity. Eigenvalues of $\hat{H}_{NH}$ are real or occur in conjugate pairs. There is also the concept of anti-pseudo-Hermiticity with a negative sign on the right hand side of eq. 103.

D. Combinations of non-Hermitian symmetries

Combinations of multiple non-Hermitian symmetries impose constraints on the eigenvalues and eigenvectors of a non-Hermitian Hamiltonian is useful for categorizing and understang them. For example, from ref. [40],

$$\hat{H}_{NH}^{comb} = \begin{bmatrix} a & b & \lambda_+ & c_+ \\ b^* & -a^* & c_+^* & -\lambda_+ \\ \lambda_- & c_- & a^* & b \\ c_-^* & -\lambda_- & b^* & -a \end{bmatrix}, \tag{104}$$

with $a, b, c_\pm \in \mathbb{C}$ and $\lambda_\pm \in \mathbb{R}$. With $\Sigma_\mu = \sigma_1 \otimes \sigma_\mu$, $\mu = 0, 1, 2, 3$, the complex conjugation operator, $\hat{\mathcal{T}}$. We can show anti-$\mathcal{PT}-$ *symmetry* with $\{\Sigma_3\Sigma_1\hat{\mathcal{T}}, \hat{H}_{NH}^{comb}\} = 0$ and pseudo-Hermiticity $\Sigma_0\hat{H}_{NH}^{comb}\Sigma_0 = \hat{H}_{NH}^{comb,\dagger}$. From this we learn, the eigenvalues either is a set $\{E, E^*, -E, -E^*\}$ with non-real E, or two real pairs, $\{E_1, -E_1\}$ and $\{E_2, -E_2\}$(orthogonal eigenstates in each pair).

1. Two Level

2. Lattice

Functions to form the lattice from the k-space Hamiltonian?

E. Non Hermitian Chern number

1. Topological Band theory of NHH

A topological band theory for NHHs was developed in [41]. The notion of gaps were extended to the complex plane of eigenenergies in NHHs along with the introduction of a classification of topologically distict "gapped" band structures. NHH bands with nonzero Chern numbers in 2d were found to possess edge states and a range of energies connecting the bulk bands in the complex plane. Curiously, a topological invariant was discovered from the energy dispersion, instead of the Bloch wavefunction. The first conceptualization or realization of exceptional points in 2d band structures was reported in that distinct gapped phases connect via an intermediate phase with band degenracies at isolated points in momentum space.

The definition of Chern numbers, Berry connection and curvature do not change from eq. 56 and the associated discussion for the Hermitian Hamiltonians. Definitions of gapped, fully gapped, and gapless bands from hermitian Hamiltonians is generalized to separable, isolated, and inseparable bands respectively. A band n is separable if its energy $E_n(\mathbf{k}) \neq \mathbf{E_m}(\mathbf{k})$ for all $m \neq n$ and all $\mathbf{k}$. An isolated band n has $E_n(\mathbf{k}) \neq \mathbf{E_m}(\mathbf{k}')$, $\forall m \neq n$, and $\mathbf{k}, \mathbf{k}'$. A band is inseparable if it is degenerate with another band at some momentum. Ref. [41] proved the four Chern numbers LL, LR, RL, and RR constituted from the L(left) and R(right) eigenstates (sharing a common eigenvalue E_n) to be equal. In Berry curvature, $i\langle\partial_i\psi_n^\alpha(\mathbf{k})|\partial_\mathbf{j}\psi_\mathbf{n}^\beta(\mathbf{k})\rangle$, $\alpha, \beta = L, R$ and n is the band index.

$$H|\psi_n^R\rangle = E_n|\psi_n^R\rangle, \quad H^\dagger|\psi_n^L\rangle = E_n^*|\psi_n^L\rangle$$

With a domain wall setup where two semi-infinte domains are separated by a wall along the y-axis, a topologically protected edge state localized at the wall was found for tow topologically distict phases of the NHH (a generalized version of 2d Dirac fermion model):

$$H^{1,N}(k_x, k_y) = (k_x + i\kappa_x)\sigma_x + (k_y + i\kappa_y)\sigma_y + (m + i\delta)\sigma_z \quad (105)$$

with $\kappa \equiv (\kappa_\mathbf{x}, \kappa_\mathbf{y})$, $\mathbf{k} \equiv (\mathbf{k_x}, \mathbf{k_y})$, $k \equiv |\mathbf{k}|$, and $\kappa \equiv |\kappa|$, the complex eigenenergies of the NHH in eq. 105 is found to be,

$$E_\pm(\mathbf{k}) = \pm\sqrt{\mathbf{k^2} - \kappa^2 + \mathbf{m^2} - \delta^2 + \mathbf{2i}(\mathbf{k}.\kappa + \mathbf{m}\delta)}, \quad (106)$$

The two bands are "separable" according to the definition for $\kappa < |m|$. The two topologically distict phases (having differing Chern numbers) with $\kappa < m$ and $-\kappa > m$ (both phases with separable two bands) separated by the domain wall lead to a band of edge state energies (complex) in the "gapped region" that connect the bulk bands.

A second NHH which support edge states localized in the interface was forwarded,

$$H^{2,N}(k_x, k_y) = (\sin k_x + i\kappa_x)\sigma_x + (\sin k_y + i\kappa_y)\sigma_y + (\cos k_x + \cos k_y + m + i\delta)\sigma_z \quad (107)$$

If we expand the NHH $H^{2,N}$ in eq. 107 around the $(k_x, k_y) = (0, 0)$ point to the lowest (linear) order we get $H^{1,N}$ in eq. 105, the continuum limit. This connection becomes important in the non-Bloch theory of Chern numbers soon forwarded in [42]. Ref. [41] also introduces the topological invariant called vorticity for a pair of complex bands called vorticity. For a closed loop Γ in momentum space, for complex bands $E_m(\mathbf{k})$ and $E_n(\mathbf{k})$,

$$\nu_{mn}(\Gamma) = -\frac{1}{2\pi}\oint_\Gamma \nabla_\mathbf{k} \arg[E_m(\mathbf{k}) - \mathbf{E_n}(\mathbf{k})].\mathbf{dk} \quad (108)$$

For a contractible loop Γ in BZ, a nonzero vorticity implies the degenracy of bands in the region enclosed by Γ. For a pair of separable bands, vorticity is alway 0 on a contractible loop. For a pair of separable bands, nonzero vorticity is found only on noncontractible loops. This leads to a $(Z/2)^d$ classification of d-dimensional separable bands. This is in contrast with gapped one dimensional Hermitian Hamiltonians who are necessarily topologically trivial. But separable non-Hermitian Hamiltonians in 1d have this $\mathbf{Z/2}$ classification.

For 2d, it is known that Hermitian Hamiltonians can not have robust degenracies without some symmetry. For example, the band degenracy in the Dirac point for 2d is unstable without additional symmetry present. On the other hand, the Weyl point in three dimensions is topologically stable. For 3d Weyl points, finding the degeneracy requires tuning three parameters. Surprisingly, for NHHs, finding degeneracy requires tuning two parameters. Furthermore, NHH at the generic degeneracy points are called defective meaning that the eigenstates do not span the full Hilbert space. Near such a defective point, the k.p Hamiltonian can be written,

$$H(\mathbf{k}) = \mathbf{aI} + \epsilon\sigma_+ + \sum_{\mathbf{i,j}} \mathbf{k_i c_{ij}} \sigma_\mathbf{j} \quad , \quad (109)$$

where i=x,y, j=x,y,z,a,ϵ and c_{ij} are complex numbers. The eigenenergies form the band,

$$E_\pm(\mathbf{k}) = \mathbf{a} \pm \sqrt{\mathbf{c_x k_x} + \mathbf{c_y k_y}}, \quad (110)$$

with $c_x = 2\epsilon(c_{xx} + ic_{xy})$, and $c_y = 2\epsilon(c_{yx} + ic_{yy})$. For $\epsilon \neq 0$, the degeneracy is defective. For $c_x, c_y \neq 0$ and $Im(c_y/c_x) \neq 0$, the band degeneracy is called "exceptional point". Exceptional points are found in inseparable intermediate phase in topological phase transitions in two dimensions. For example, for the Hamiltonian $H^{1,N}$ in eq. 105, the two topologically distinct regions $m > \kappa$

and $m < -\kappa$ are separated by the intermediate regime $|m| < |\kappa|$. In this intermediate region, the two bands $E_\pm(\mathbf{k})$ cross at two isolated points $\mathbf{k}_\pm$ (the exceptional points) in the momentum space,

$$\mathbf{k}_\pm = -\frac{\mathbf{m}\delta}{\kappa}\hat{\mathbf{n}} \pm \frac{\sqrt{(\boldsymbol{\kappa}^{\mathbf{2}} - \mathbf{m}^{\mathbf{2}})(\boldsymbol{\kappa}^{\mathbf{2}} + \boldsymbol{\delta}^{\mathbf{2}})}}{\kappa}\hat{\mathbf{z}} \times \hat{\mathbf{n}}, \quad (111)$$

$\hat{n} = \kappa/|\kappa|$. The separable band structures($|m| > \kappa$) have zero total vorticity. The two exceptional points have opposite vorticities. The Hamiltonian is defective at the degeneracy points. Non Hermitian phase transitions occur through these exceptional point pairs.

2. Non-Hermitian Chern bands

Ref. [42] introduces a non-Bloch chern number that accurately predicts the number of chiral edge modes whereas chern nmbers from a non Hermitian bloch hamiltonian fails. From the non-hermitian Hamiltonian $H^{Bloch}(\mathbf{k})$, the algorithm proceeds in a couple of steps: 1) find the low energy continuum model of $H^{Bloch}(\mathbf{k})$ around a local minima $H(\mathbf{k})$ (the issue not really investigated), a linear or quadratic in $\mathbf{k}$ expansion can be taken, 2) find the "Non-Bloch" Hamiltonian: $\tilde{H}(\tilde{\mathbf{k}}) \equiv H(\mathbf{k} \to \tilde{\mathbf{k}} + \mathbf{i}\tilde{\mathbf{k}}')$. $\tilde{\mathbf{k}}'$ is, in general, a function of $\tilde{\mathbf{k}}$. $\tilde{\mathbf{k}}$ parametrizes the generalized Brillouin Zone $\tilde{T}^2(\tilde{\mathbf{k}})$, a deformation of the original Brillouin Zone $T^2(\tilde{\mathbf{k}})$ into complex spaces. The non-Bloch Chern number is defined as the standard chern number of $\tilde{H}(\tilde{\mathbf{k}})$ (instead of $H(\mathbf{k})$). Ref. [42] also demonstrates a NHH model where the continuum limit was not taken and the chern number was calculated from step 2 alone. Also their definition of chern number is with left and right eigenvectors in the way written out below:

$$\tilde{H}(\tilde{\mathbf{k}})|u_{R\alpha}\rangle = E_\alpha|u_{R\alpha}\rangle, \quad \tilde{H}^\dagger(\tilde{\mathbf{k}})|u_{L\alpha}\rangle = E^*_\alpha|u_{L\alpha}\rangle, \quad \langle u_{L\alpha}|u_{R\alpha}\rangle = 1 \quad (112)$$

$$C_{(\alpha)} = \frac{1}{2\pi i}\int_{\tilde{T}^2} d^2\tilde{\mathbf{k}}\epsilon^{ij}\langle\partial_i u_{L\alpha}(\tilde{\mathbf{k}})|\partial_j u_{R\alpha}(\tilde{\mathbf{k}})\rangle \quad (113)$$

$\tilde{H}(\tilde{\mathbf{k}}) = VJV^{-1}$, J is diagonal, every column of V($(V^\dagger)^{-1}$) is a right(left) eigenvector with normalization $\langle u_{L\alpha}|u_{R\beta}\rangle = \delta_{\alpha\beta}$. $\epsilon^{xy} = -\epsilon^{yx} = 1$. Eq. 113 yields the correct number of chiral edge modes. Eq. 112 is called the biorthogonal normalization [43] and the Berry phase in eq. 113 the global biorthogonal Berry phase [44]. As is done in many cases, an alternate expression for C_α is,

$$C_\alpha = \frac{1}{2\pi i}\int_{\tilde{T}^2} d^2\tilde{\mathbf{k}}\epsilon^{ij}Tr(P_\alpha\partial_i P_\alpha\partial_j P_\alpha), \quad (114)$$

where $P_\alpha = |u_{R\alpha}(\tilde{\mathbf{k}})\rangle\langle u_{L\alpha}(\tilde{\mathbf{k}})|$ is the projection operator defined with a specific arrangement of L and R.

The NHH demonstrated in ref. [42] can be obtained from $H^{2,N}(k_x, k_y)$ in eq. 107 with $t \to \nu_x$, $t \to \nu_x$ and generalizing with parameters t_x, t_ys. With the expansion to k_j^2 order, ($H^{2,N}(k_x, k_y)$ in eq. 105 was to k_j order or linear order)

$$H(\mathbf{k}) = (\nu_{\mathbf{x}}\mathbf{k}_{\mathbf{x}} + \mathbf{i}\gamma_{\mathbf{x}})\sigma_{\mathbf{x}} + (\nu_{\mathbf{y}}\mathbf{k}_{\mathbf{y}} + \mathbf{i}\gamma_{\mathbf{y}})\sigma_{\mathbf{y}} + \left(m - t_x - t_y + \frac{t_x}{2}k_x^2 + \frac{t_y}{2}k_y^2\right)\sigma_z \quad (115)$$

$$\tilde{H}(\tilde{\mathbf{k}}) \equiv H(\mathbf{k} \to \tilde{\mathbf{k}} + \mathbf{i}\tilde{\mathbf{k}}') \quad (116)$$

Using the transformation eq. 116, the Hamiltonian $H(\mathbf{k})$ is turned into,

$$\tilde{H}(\tilde{\mathbf{k}}) = \nu_x\tilde{k}_x\sigma_x + \nu_y\tilde{k}_y\sigma_y + \left(\tilde{m} + \frac{t_x\tilde{k}_x^2 + t_y\tilde{k}_y^2}{2} - i\sum_j \frac{t_j\gamma_j\tilde{k}_j}{\nu_j}\right)\sigma_z, \quad (117)$$

with $\tilde{m} = m - t_x - t_y - \frac{t_x\gamma_x^2}{2\nu_x^2} - \frac{t_y\gamma_y^2}{2\nu_y^2}$, which is used for the Chern number calculation.

Because of adaptibility to analytical work, the following model is useful,

$$H^A(\mathbf{k}) = \sin(\mathbf{k}_{\mathbf{x}} + \mathbf{i}\gamma_{\mathbf{x}})\sigma_{\mathbf{x}} + \sin(\mathbf{k}_{\mathbf{y}} + \mathbf{i}\gamma_{\mathbf{y}})\sigma_{\mathbf{y}} + [m - t\cos(k_x + i\gamma_x) - t\cos(k_y + i\gamma_y)]\,\sigma_z \quad (118)$$

$$H^A(x,y) = \sum_x c_x^\dagger(m\sigma_z)c_x + \sum_x c_x^\dagger\sum_{j=x,y}\frac{\exp(-\gamma_j)}{2}(-i\sigma_j - t\sigma_z)c_{x+e_j} + \sum_x c_x^\dagger\sum_{j=x,y}\frac{\exp(\gamma_j)}{2}(i\sigma_j - t\sigma_z)c_{x-e_j}, \quad (119)$$

where $\mathbf{x} = (\mathbf{x}, \mathbf{y})$ are the integer coordinates of unit cells, $c_{\mathbf{x}} = (c_{\mathbf{x},\mathbf{A}}, c_{\mathbf{x},\mathbf{B}})^T$ is a two-component annihilation operator, $\hat{e}_j$ is the unit vector along the j direction. $H^A(x,y)$ can be diagonalized subject to OBC on a square of side L. $H^A(x,y)$ becomes a $2L^2 \times 2L^2$ matrix. If $|\psi\rangle$ is a eigenvector, then with a diagonal matrix S with elements $S(x,y) = exp(\gamma_x x + \gamma_y y)$, we can find,

$$H|\psi\rangle = E|\psi\rangle$$
$$\bar{H}|\bar{\psi}\rangle = E|\bar{\psi}\rangle$$
$$|\bar{\psi}\rangle = S^{-1}|\psi\rangle$$
$$\bar{H} = S^{-1}HS$$

Interestingly, the $\mathbf{k}$-space Hamiltonian of $\bar{H}$ is the Qi-Wu-Zhang model [45]. Standing wave excitations are signatures of Open Boundary Conditions. For the OBCs we take the transformations, $\mathbf{k} \to \tilde{\mathbf{k}} + \mathbf{i}\tilde{\mathbf{k}}'$, with $\tilde{\mathbf{k}}' = (-\gamma_x, -\gamma_y)$.

Then,

$$\tilde{H}(\tilde{\mathbf{k}}) = \sin(\tilde{k}_x)\sigma_x + \sin(\tilde{k}_y)\sigma_y \left[m - t\cos(\tilde{k}_x) - t\cos(\tilde{k}_y)\right]\sigma_z \quad (120)$$

The non-Bloch chern number of $H(\mathbf{k})$ is simply the usual chern number of $\tilde{H}(\tilde{\mathbf{k}})$.

Appendix A: Spin chain

$$\hat{H} = -\sum_{l=0}^{L-1}\left[\hat{b}_l^\dagger \hat{b}_{l+1} + \hat{b}_l \hat{b}_{l+1}^\dagger + \frac{\Delta}{2}\left(2\hat{n}_l - 1\right)\left(2\hat{n}_{l+1} - 1\right)\right], \quad \text{(A1)}$$

With $\left(\hat{b}_l^\dagger\right)^2 = \left(\hat{b}_l\right)^2 = 0$.

1. Block Diagonalization

2. Particle Number Conservation

$$H = H_0 \oplus H_1 \oplus ... \oplus H_N \oplus ... \oplus H_L \quad \text{(A2)}$$

3. Translational Symmetry

$$\begin{bmatrix} |0011, k=0\rangle \\ |0101, k=0\rangle \\ |0011, k=1\rangle \\ |0011, k=3\rangle \\ |0101, k=2\rangle \\ |0011, k=2\rangle \end{bmatrix} = U \begin{bmatrix} |0011\rangle \\ |0101\rangle \\ |0110\rangle \\ |1001\rangle \\ |1010\rangle \\ |1100\rangle \end{bmatrix} \quad \text{(A3)}$$

where,

$$U = \begin{bmatrix} \frac{1}{2}\omega_0^0 & 0 & \frac{1}{2}\omega_0^{-1} & \frac{1}{2}\omega_0^{-3} & 0 & \frac{1}{2}\omega_0^{-2} \\ 0 & \frac{1}{2\sqrt{2}}\left(\omega_0^0 + \omega_0^{-2}\right) & 0 & 0 & \frac{1}{2\sqrt{2}}\left(\omega_0^{-1} + \omega_0^{-3}\right) & 0 \\ \frac{1}{2}\omega_1^0 & 0 & \frac{1}{2}\omega_1^{-1} & \frac{1}{2}\omega_1^{-3} & 0 & \frac{1}{2}\omega_1^{-2} \\ \frac{1}{2}\omega_3^0 & 0 & \frac{1}{2}\omega_3^{-1} & \frac{1}{2}\omega_3^{-3} & 0 & \frac{1}{2}\omega_3^{-2} \\ 0 & \frac{1}{2\sqrt{2}}\left(\omega_2^0 + \omega_2^{-2}\right) & 0 & 0 & \frac{1}{2\sqrt{2}}\left(\omega_2^{-1} + \omega_2^{-3}\right) & 0 \\ \frac{1}{2}\omega_2^0 & 0 & \frac{1}{2}\omega_2^{-1} & \frac{1}{2}\omega_2^{-3} & 0 & \frac{1}{2}\omega_2^{-2} \end{bmatrix}$$

4. Unitary Transformation

$$UU^\dagger = \mathbf{1} \quad \text{(A4)}$$

$$UH_{N=2}U^\dagger = \begin{bmatrix} 0 & -2\sqrt{2} & 0 & 0 & 0 & 0 \\ -2\sqrt{2} & 2\Delta & 0 & 0 & 0 & 0 \\ 0 & 0 & 0 & 0 & 0 & 0 \\ 0 & 0 & 0 & 0 & 0 & 0 \\ 0 & 0 & 0 & 0 & 2\Delta & 0 \\ 0 & 0 & 0 & 0 & 0 & 0 \end{bmatrix}$$

$$\begin{bmatrix} 0 & -2\sqrt{2} & 0 & 0 & 0 & 0 \\ -2\sqrt{2} & 2\Delta & 0 & 0 & 0 & 0 \\ 0 & 0 & 0 & 0 & 0 & 0 \\ 0 & 0 & 0 & 0 & 0 & 0 \\ 0 & 0 & 0 & 0 & 2\Delta & 0 \\ 0 & 0 & 0 & 0 & 0 & 0 \end{bmatrix}$$

$$UHU^\dagger\left(U\psi\right) = \epsilon\left(U\psi\right) \quad \text{(A5)}$$

So, after finding the eigenvectors $(U\psi)$ in the transformed basis, we get back eigenvectors in the original basis by pre-multiplying $(U\psi)$ with $U^\dagger$.

5. k=0 block only

Now,

$$U_{k-0}H_{N=2}U_{k=0}^\dagger = \begin{bmatrix} 0 & -2\sqrt{2} \\ -2\sqrt{2} & 2\Delta \end{bmatrix}$$

Appendix B: Mapping problems in Lattice Models with QuTiP

Polariton spectrum of the Dicke-Ising model [14].

$$H_M = \sum_{n=1}^{N}\omega_0\sigma_n^+\sigma_n^- + J\sum_{n=1}^{N-1}\left(\sigma_n^+ + \sigma_n^-\right)\left(\sigma_{n+1}^+ + \sigma_{n+1}^-\right) \quad \text{(B1)}$$

```
cells = 40
cell_num_site = 1
cell_site_dof = [2]
J = 2
omega0 = 2
H_cell_s = tensor(omega0 * sigmap() * sigmam(),
    qeye(2))
inter_cell_T0 = J* sigmap() + J* sigmap() *
    sigmam()
inter_cell_T_s = tensor(inter_cell_T0, qeye(2))
Spin_lattice = Lattice1d(num_cell=cells,
    boundary = "periodic", cell_num_site = 1,
    cell_site_dof = [4], Hamiltonian_of_cell =
    H_cell_s, inter_hop = inter_cell_T_s)
Spin_lattice.plot_dispersion()
```

Listing 30. Python example

Alternately, the spectrum can be found from diagonalizing the Hamiltonian.

```
SHam = Spin_lattice.Hamiltonian()
Es = SHam.eigenenergies()
ind_l = np.arange(0, 2*cells, 1, dtype=int)
fig, ax = plt.subplots()
ax.plot(ind_l, Es[0:2*cells] )
```

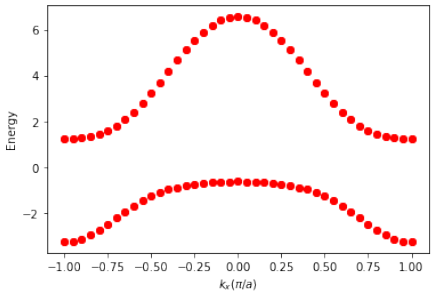

FIG. 8. Dispersion in the spin lattice model.

```
ax.plot(ind_l, Es[2*cells:4*cells] )
ax.set_ylabel('Eigenvalue')
ax.set_xlabel('Eigenvalue index')
plt.show(fig)
```

Listing 31. Python example

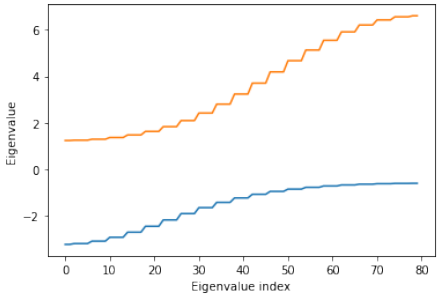

FIG. 9. Eigenvalues of the Hamiltonian of the spin lattice.

1. The Bose Approximation

$$H_M = \sum_{n=1}^{N} \omega_0 b_n^\dagger b_n + J \sum_{n=1}^{N-1} \left(b_n^\dagger + b_n\right)\left(b_{n+1}^\dagger + b_{n+1}\right) \tag{B2}$$

```
cells = 4
cell_num_site = 1
cell_site_dof = [2]
J = 2
omega0 = 2
N = cells     # number of sites/modes
Np = 4   # bosonic hilbert space dimension
H_cell_b = omega0 * create(Np) * destroy(Np)
inter_cell_T_b = J* create(Np) * destroy(Np)
Bose_lattice = Lattice1d(num_cell=cells,
    boundary = "periodic", cell_num_site = 1,
    cell_site_dof = [Np], Hamiltonian_of_cell =
    H_cell_b, inter_hop = inter_cell_T_b )
Bose_lattice.plot_dispersion()
```

Listing 32. Python example

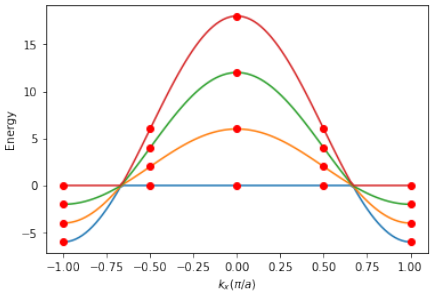

FIG. 10. Dispersion of the spin lattice model in the bose approximation.

2. The Jordan Wigner Transformation

The Jordan Wigner transformation,

$$\sigma_n^- = \Pi_{j<n}\left(1 - 2c_j^\dagger c_j\right) c_n$$
$$\sigma_n^+ = \Pi_{j<n}\left(1 - 2c_j^\dagger c_j\right) c_n^\dagger$$

yields the fermionic Hamiltonian,

$$H_F = \sum_{n=1}^{N} \omega_0 c_n^\dagger c_n + J \sum_{n=1}^{N-1} \left(c_n^\dagger c_{n+1} - c_n c_{n+1}^\dagger\right) + J \sum_{n=1}^{N-1} \left(c_n^\dagger c_{n+1}^\dagger - c_n c_{n+1}\right) \tag{B3}$$

```
cells = 4
cell_num_site = 1
cell_site_dof = [2]
J = 2
omega0 = 2
H_cell_f = omega0/2 * (1+sigmaz())
inter_cell_T_f = J* sigmap()* sigmam() + J*
    sigmap()
Fermion_lattice = Lattice1d(num_cell=cells,
    boundary = "periodic", cell_num_site = 1,
    cell_site_dof = [2], Hamiltonian_of_cell =
    H_cell_f, inter_hop = inter_cell_T_f )
Fermion_lattice.plot_dispersion()
```

Listing 33. Python example

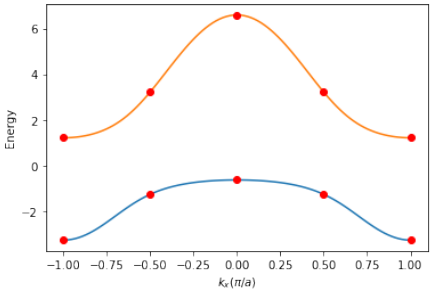

FIG. 11. Dispersion of the fermion lattice model in the Jordan Wigner approximation.

This model has analytical solution.

$$H_F = \sum_k E_{F,k} d^\dagger_{F,k} d_{F,k} + E^0_F \tag{B4}$$

The $d_{F,k}, d^\dagger_{F,k}$ operators follow the Fermionic anticommutation relationships.

$$\{d_{F,k}, d^\dagger_{F,k}\} = \delta_{k,k}, \quad \{d^\dagger_{F,k}, d^\dagger_{F,k}\} = \{d_{F,k}, d_{F,k}\} = 0$$

With k being the quasi-momentum in the range $0 < k < \pi$,

$$E_{F,k} = \sqrt{\omega_0^2 + 4J^2 + 4J\omega_0 \cos k}, \tag{B5}$$

with the ground state energy,

$$E^0_F = \frac{1}{2}\left(N\omega_0 - \sum_k E_{F,k}\right) \tag{B6}$$

3. The Holstein-Primakoff transformation

$$\sigma^+_n = b^\dagger_n \sqrt{1 - b^\dagger_n b_n} = b^\dagger_n \left(1 - \frac{1}{2} b^\dagger_n b_n - \frac{1}{8} b^\dagger_n b_n b^\dagger_n b_n\right)$$
$$\sigma^-_n = \sqrt{1 - b^\dagger_n b_n} b_n = \left(1 - \frac{1}{2} b^\dagger_n b_n - \frac{1}{8} b^\dagger_n b_n b^\dagger_n b_n\right) b_n$$

$$H^{(0)}_M = \sum_{n=1}^{N} \omega_0 b^\dagger_n b_n + J \sum_{n=1}^{N-1} \left(b^\dagger_n + b_n\right)\left(b^\dagger_{n+1} + b_{n+1}\right)$$

$$H^{(1)}_M = -\frac{J}{2} \sum_{n=1}^{N-1} b^\dagger_n \left\{\left(b^\dagger_n + b_n\right)\left(b^\dagger_{n-1} + b_{n-1} + b^\dagger_{n+1} + b_{n+1}\right)\right\}$$

```
cells = 4
cell_num_site = 1
J = 2
omega0 = 2
N = cells    # number of sites/modes
Np = 4   # bosonic hilbert space dimension
cell_site_dof = [Np]
H_cell_hp = omega0/2 * tensor(qeye(2), num(Np))
eta = tensor( sigmaz(), qeye(Np))
inter_cell_T_hp = J * tensor(sigmap() * sigmam()
    , num(Np)) + J * tensor(sigmap(), num(Np))
hp_boson_lattice = Lattice1d(num_cell=cells,
    boundary = "periodic", cell_num_site = 2,
    cell_site_dof = [Np], Hamiltonian_of_cell =
    H_cell_hp, inter_hop = inter_cell_T_hp )
hp_boson_lattice.plot_dispersion(bose_d=1)
```

Listing 34. Python example

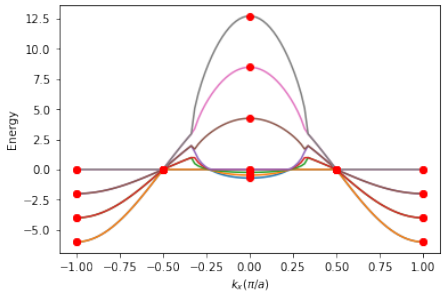

FIG. 12. Dispersion of the boson lattice model in the first order Holstein-Primakoff approximation.

Appendix C: Bethe Ansatz example

For two electron wavefunctions, with one spin-down and one spin-up electrons, the Lieb-Wu equations are of the form [46],

$$e^{ik_j L} = \frac{\Lambda - sin(k_j) - iu}{\Lambda - sin(k_j) + iu}, \quad j = 1, 2$$
$$1 = \Pi^2_{j=1} \frac{\Lambda - sin(k_j) - iu}{\Lambda - sin(k_j) + iu} \tag{C1}$$

$$\begin{aligned}
&\psi(x_1, x_2; \downarrow, \uparrow | k_1, k_2; \Lambda) \\
&= \Theta_H(x_2 - x_1)\left[\frac{2iue^{ik_1x_1 + ik_2x_2}}{\Lambda - sin(k_1) + iu} - \frac{2iue^{ik_2x_1 + ik_1x_2}}{\Lambda - sin(k_2) + iu}\right] \\
&+\Theta_H(x_1 - x_2)\left[\frac{2iue^{ik_1x_1 + ik_2x_2}}{\Lambda - sin(k_1) + iu} \cdot \frac{\Lambda - sin(k_2) - iu}{\Lambda - sin(k_2) + iu}\right. \\
&\left. - \frac{2iue^{ik_2x_1 + ik_1x_2}}{\Lambda - sin(k_2) + iu} \cdot \frac{\Lambda - sin(k_1) - iu}{\Lambda - sin(k_1) + iu}\right]
\end{aligned} \tag{C2}$$

```
L= 4;
uP = 0.25;
k1,k2,lamda=sym.symbols('k1 k2 lamda')
fval0= exp(I * k1 * L)- (lamda - sin(k1) - I *
    uP)/(lamda - sin(k1) + I * uP)
fval1= exp(I * k2 * L)- (lamda - sin(k2) - I *
    uP)/(lamda - sin(k2) + I * uP)
fval2= 1 - (lamda - sin(k1) - I * uP)/(lamda -
    sin(k1) + I * uP) * (lamda - sin(k2) - I *
    uP)/(lamda - sin(k2) + I * uP)
fval_C=sym.Matrix([[fval0], [fval1], [fval2]])
jacb=sym.Matrix([[diff(fval0,k1),diff(fval0,k2),
    diff(fval0,lamda)],
      [diff(fval1,k1),diff(fval1,k2),diff(fval1,
    lamda)],
      [diff(fval2,k1),diff(fval2,k2),diff(fval2,
    lamda)]])
i_jacb = jacb.inv()
i_jacb_C = i_jacb * fval_C
ini_G = sym.Matrix([[2.668*pi/3],[1.8317*pi
    /3],[0.6004]]).evalf()
err_C = ini_G

Cols = ini_G
Cols_prv = ini_G
TotalIters = 200
```

```
tolerance = 1e-12
for i in range(TotalIters):
    i_jacb_C_vals = i_jacb_C.subs([(k1, Cols[0])
    , (k2, Cols[1]), (lamda, Cols[2])])

    Cols = Cols - i_jacb_C_vals.evalf()
    err = np.abs(Cols-Cols_prv)/ np.abs(Cols_prv
    )
    if np.mod(i,2) == 1:
        print('i: ',i,' err: ',err)
    if np.max(err) < tolerance:
        break
    Cols_prv = Cols

k1s = Cols[0]
k2s = Cols[1]
lamdas = Cols[2]

k1s=complex(k1s.evalf())
k2s=complex(k2s.evalf())
lamdas=complex(lamdas.evalf())
```

Listing 35. Python example

```
fermiHubbardLattice1d = Lattice1d_fermi_Hubbard(
    num_sites=L, boundary="periodic", t=1, U=1,
    V=0)
fillingUp = 1
fillingDown = 1
[Hamiltonian, basisStatesUp, basisStatesDown,
    normHubbardStates] = fermiHubbardLattice1d.
    Hamiltonian(fillingUp=fillingUp, fillingDown
    =fillingDown)

nbasisStatesUp = np.shape(basisStatesUp)[0]
nbasisStatesDown = np.shape(basisStatesDown)[0]

num21 = lamdas - np.sin(k2s) - 1j*uP
num22 = lamdas - np.sin(k1s) - 1j*uP
den1 = lamdas - np.sin(k1s) + 1j*uP
den2 = lamdas - np.sin(k2s) + 1j*uP
den12 = den1*den2

psi_r = np.zeros((nbasisStatesDown *
    nbasisStatesUp, 1), dtype=complex)
kx_o = np.zeros((nbasisStatesDown *
    nbasisStatesUp, 1), dtype=complex)
kx_c = np.zeros((nbasisStatesDown *
    nbasisStatesUp, 1), dtype=complex)

r = -1
for u in range(nbasisStatesUp):
#for u in range(1,2,1):
    x2 = np.argwhere(basisStatesUp[u, :])
    x2 = x2[0, 0]
#    for d in range(0,1,1):
    for d in range(nbasisStatesDown):
        x1 = np.argwhere(basisStatesDown[d, :])
        x1 = x1[0, 0]

#         print(x1, x2)
        r = r + 1
        kx_o[r] = 1j*(k1s*x1+k2s*x2)
        kx_c[r] = 1j*(k1s*x2+k2s*x1)

        psi_r[r] = np.heaviside(x2-x1, 0.5)* 2j*
    uP*(np.exp(kx_o[r])/den1 - np.exp(kx_c[r])/
    den2)\
    +np.heaviside(x1-x2,0.5)*2j*uP*(np.exp(kx_o[
    r])/den12*num21-np.exp(kx_c[r])/den12*num22)
        print(psi_r[r])

psi = psi_r/np.sqrt(np.sum(np.multiply(psi_r, np
    .conj(psi_r))))
```

Listing 36. Python example

Appendix D: Simulating Fermi-Hubbard model with two component hardcore Bose Hubbard model

[47] illustrates a Bose-Hubbard model for two species that can realize a number of curious phenomena that fermions manifest.

For a gas consisting of N bosonic atoms with two internal levels denoted by $\uparrow,\downarrow$ in a one-dimensional optical lattice with M wells (filling factor of $\nu = N/2M$), the Hamiltonian is [48]

$$H = -t\sum_{\langle i,j\rangle} a^\dagger_{i\sigma}a_{j\sigma} + U\sum_{i,\sigma} a^\dagger_{i\sigma}a_{i\sigma}a^\dagger_{i\sigma}a_{i\sigma} + V\sum_i a^\dagger_{i\uparrow}a_{i\uparrow}a^\dagger_{i\downarrow}a_{i\downarrow} \tag{D1}$$

$a^\dagger_{i\sigma}(a_{i\sigma})$ creates(destroys) an atom on i-th lattice site with spin σ. t,U,V can be written in terms of measurable physical parameters. A notation is adopted for the states,

$$|\mathbf{x},\mathbf{y}\rangle = \mathbf{a^\dagger_{x_1,\uparrow}a^\dagger_{x_2,\uparrow}....a^\dagger_{x_{N_\uparrow},\uparrow}a^\dagger_{y_1,\downarrow}a^\dagger_{y_2,\downarrow}....a^\dagger_{y_{N_\downarrow},\downarrow}|vac\rangle, \tag{D2}$$

with $N_\uparrow + N_\downarrow = N$, $\mathbf{x} = (\mathbf{x_1},...,\mathbf{x_{N_\uparrow}})$, and $\mathbf{y} = (\mathbf{y_1},...,\mathbf{y_{N_\downarrow}})$ denote, respectively, the site indices occupied by spin up and down particles. With the limit $U\to\infty$, we can facilitate $x_i \neq x_j, y_i \neq y_j, \forall i \neq j$. It is equivalent of dropping the U term altogether.

$$H = -t\sum_{\langle i,j\rangle} a^\dagger_{i\sigma}a_{j\sigma} + V\sum_i a^\dagger_{i\uparrow}a_{i\uparrow}a^\dagger_{i\downarrow}a_{i\downarrow} \tag{D3}$$

$$|\Psi_B\rangle = \sum_{x,y} f_B(x,y)|\mathbf{x},\mathbf{y}\rangle \tag{D4}$$

With the Jordan Wigner transformation,

$$a^\dagger_{i\sigma} = (-1)^{\sum_{j<i}(1-2c^\dagger_{j\sigma}c_{j\sigma})}c^\dagger_{i\sigma} \tag{D5}$$

the bosonic Hamiltonian in eq. D3 is transformed exactly to a Fermi Hubbard model (eq. 30) with on-site interaction U=V.

$$H = -t\sum_{\langle i,j\rangle} c^\dagger_{i\sigma}c_{j\sigma} + U\sum_i c^\dagger_{i\uparrow}c_{i\uparrow}c^\dagger_{i\downarrow}c_{i\downarrow} \tag{D6}$$

The two Hamiltonians have the same eigen-spectrum and the eigenfunctions have the correspondence:

$$|\Psi_B\rangle = \sum_{x,y} f_B(x,y)|\mathbf{x},\mathbf{y}\rangle \to |\mathbf{\Psi_F}\rangle = \sum_{\mathbf{x},\mathbf{y}} \mathbf{f_F}(\mathbf{x},\mathbf{y})|\mathbf{x},\mathbf{y}\rangle_\mathbf{F}$$

The coefficients are related by,

$$f_B(x,y) = sgn(x,y)f_F(x,y)$$
$$= \Pi_{i<j}sgn(x_i-x_j)sgn(y_i-y_j)f_F(x,y)$$

$|\mathbf{x},\mathbf{y}\rangle_\mathbf{F}$ is defined in eq.29.

Appendix E: Spin-1/2 in a magnetic field

The quintessential example of nontrivial topology is the motion of spin-1/2 particle in a magnetic field.

```
N = 50
thetas = np.linspace(0, np.pi, N)
phis = np.linspace(0, 2*np.pi, N)
eigfs = np.zeros((N, N, 2, 2), dtype=complex)
for i in range(N):
    for j in range(N):
        # H = B.sigma, sigma is vector of Pauli
    matrices
        H = sigmax() * np.sin(thetas[i]) * np.
    cos(phis[j]) + sigmay() * np.sin(thetas[i])
    * np.sin(phis[j]) + np.cos(thetas[i]) *
    sigmaz()
        H = -H              #Figure this out
    please
        _, eigs = np.linalg.eigh(H)
        eigs=eigs.T         # the eigenvectors
    need to be rows in eigfs
        eigfs[i, j, :, :] = eigs[:, :]
b_curv = berry_curvature(eigfs)
plot_berry_curvature(eigfs)
print('The Chern number is:')
print(b_curv.sum()/2/np.pi)
```

Listing 37. Building Hamiltonian for 2d lattice

The chern nuber of two filled bands is 0. Nonzero chern number can be found in the gap. The only gap is between the two bands. To calculate the chern numbers of 1 filled band, the number of *occupied band*(*max_occ*) would be 1.

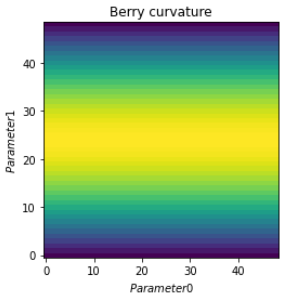

FIG. 13. Dispersion of a 2d rectangular tight binding lattice with nearest neighbour hopping only.

```
max_occ = 1
occ_bnds = np.zeros((N,N,max_occ,2),dtype=
    complex)
for i in range(max_occ):
    occ_bnds[:,:,i,:] = eigfs[:,:,i,:]
b_curv = berry_curvature(occ_bnds)
plot_berry_curvature(occ_bnds)
print('The Chern number is:')
print(b_curv.sum()/2/np.pi )
```

Listing 38. Building Hamiltonian for 2d lattice

```
print('All columns of b_curv should be
    proportional to sin(\theta)')
sinn = b_curv[:,1]
fig, ax = subplots()
```

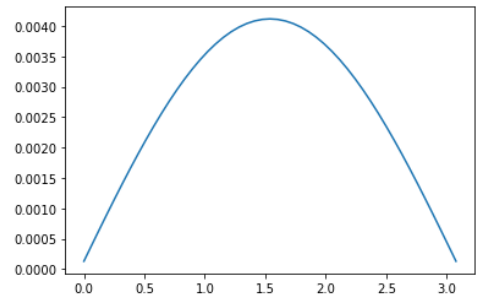

FIG. 14. Dispersion of a 2d rectangular tight binding lattice with nearest neighbour hopping only.

```
ax.plot(thetas[0:N-1], b_curv[:,5]);
show()
```

Listing 39. Building Hamiltonian for 2d lattice

For geometric phase in a dissipative teo-level system see [49]

Appendix F: Building two dimensional lattices

Two dimensional lattices are spanned by two Bravais lattice vectors and can be decomposed into separate lines/chains interconnected with links. The rectangular ('cubic') lattice is the simplest example. The Hamiltonian for a lattice in the single particle physics can be obtained very easily using tensor tools.

```
cells_x = 4
cells_y = 3
boundary_condition_x = "aperiodic"
boundary_condition_y = "periodic"
OneLayer = Lattice1d(num_cell=cells_x, boundary
    = boundary_condition_x)  # Along x axis

Hamiltonian_layer = OneLayer.Hamiltonian()
MultiLayer = Lattice1d(num_cell=cells_y,
    boundary = boundary_condition_y)
Hamiltonian_allLayer = MultiLayer.Hamiltonian()
Hamiltonian_2dlattice = tensor(
    Hamiltonian_allLayer, qeye(cells_x)) +
    tensor(qeye(cells_y), Hamiltonian_layer)
```

Listing 40. Building Hamiltonian for 2d lattice

Two-dimensional dispersions can be computed with the aid of Lattice1d instances. If the hopping are confined to two orthogonal directions, it is easier to compute. But, for the general case of hopping in two or more non-orthogonal directions may also be taken care of, with the use of *get_dispersion*() functions. The case of rectangular lattice with Next-Nearest-Neighbour (NNN) coupling (diagonally hopping in the rectangle) is given below.

```
t = 1
tp = 0.4
boundary_condition_x = "periodic"
cells_x = 30
cells_y = 30
kx_lattice = Lattice1d(num_cell=cells_x,
    boundary = boundary_condition_x)
```

```
H_k2s = np.array([[None for i in range(cells_x)] for j in range(cells_y) ])
(knxA, qH_ks, val_kns, vec_kns, vec_xs) = kx_lattice._k_space_calculations()
for ky in range(cells_y):
    boundary_condition_y = "periodic"
    site_dof = [1]
    ky_lattice = Lattice1d(num_cell=cells_y, boundary = boundary_condition_y, cell_num_site = 1, cell_site_dof = site_dof, Hamiltonian_of_cell = qH_ks[ky], inter_hop = Qobj([[-1]])     )
    (knyA, qH_k2s, val_kns, vec_kns, vec_xs) = ky_lattice._k_space_calculations()
    H_k2s[ky] = qH_k2s

Hk = np.zeros((cells_x, cells_y) ,dtype=complex)
Hk_N = np.zeros((cells_x, cells_y) ,dtype=complex)

for kx in range(cells_x):
    for ky in range(cells_y):
        Hk[kx, ky] = H_k2s[kx][ky].full()

fig, ax = plt.subplots(subplot_kw={"projection": "3d"})
X, Y = np.meshgrid(knxA, knyA)
surf = ax.plot_surface(X, Y, -t*np.real(Hk), cmap=cm.coolwarm,
                       linewidth=0, antialiased=False)

ax.set_zlim(-4, 4)
ax.zaxis.set_major_locator(LinearLocator(4))
fig.colorbar(surf, shrink=0.5, aspect=5)
ax.view_init(-15, 30)
plt.show()

X, Y = np.meshgrid(knxA, knyA)
kpxA = X + Y
kpyA = X - Y

for ikx in range(cells_x):
    for iky in range(cells_y):
        kx = knxA[ikx]
        ky = knyA[iky]

        DLT = np.argwhere(kpxA == kx)
        iArg1 = DLT[:, 0]
        DLT = np.argwhere(kpyA == ky)
        iArg2 = DLT[:, 0]
        if np.size(np.intersect1d(iArg1, iArg2)):
            AtR = np.intersect1d(iArg1, iArg2)
        a = np.abs(kpxA - kx) + np.abs(kpyA - ky)
        indx = np.unravel_index(np.argmin(a, axis=None), a.shape)
        print("(ikx, iky):  ",ikx," ",iky)
        print(" ")
        Hk_N[ikx, iky] = Hk[indx[0], indx[1]]

H_kC = -t * Hk + tp * Hk_N

fig, ax = plt.subplots(subplot_kw={"projection": "3d"})
# Plot the surface.
surf = ax.plot_surface(X, Y, np.real(H_kC), cmap=cm.coolwarm,
                       linewidth=0, antialiased=False)
ax.set_zlim(-4, 4)
ax.zaxis.set_major_locator(LinearLocator(4))
#ax.zaxis.set_major_formatter('{x:.02f}')

# Add a color bar which maps values to colors.
fig.colorbar(surf, shrink=0.5, aspect=5)
ax.view_init(-15, 30)
plt.show()
```

Listing 41. Dispersion relationships 2d lattice

Alternatively each layer may be considered a site of the Lattice1d() instance.

```
site_dof = [cells_x]
MultiLayered = Lattice1d(num_cell=cells_y, boundary = boundary_condition_y, cell_num_site = 1, cell_site_dof = site_dof, Hamiltonian_of_cell = Hamiltonian_layer, inter_hop = -t*qeye(cells_x))
Hamiltonian_2d = MultiLayered.Hamiltonian()
```

Listing 42. Building Hamiltonian for 2d lattice sitewise

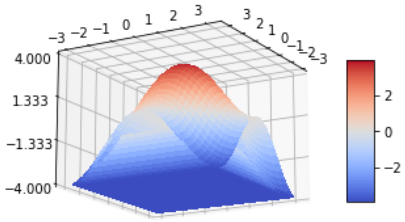

FIG. 15. Dispersion of a 2d rectangular tight binding lattice with nearest neighbour hopping only.

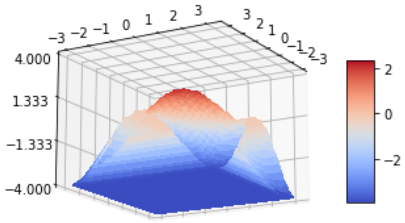

FIG. 16. Dispersion of a 2d rectangular tight binding lattice with nearest neighbour hopping of (-1) as well as next nearest neighbour hopping of 0.4.

Although, for cases like these writing the dispersion out by hand might be an easier way.

Appendix G: Exploiting additional symmetry

k=0 commutes with reflection 4.1.4 of [50]

[1] J. R. Johansson, P. D. Nation, and F. Nori, Qutip: An open-source python framework for the dynamics of open quantum systems, Computer Physics Communications **183**, 1760 (2012).

[2] A. Asenjo-Garcia, M. Moreno-Cardoner, A. Albrecht, H. Kimble, and D. E. Chang, Exponential improvement in photon storage fidelities using subradiance and selective radiance in atomic arrays, Physical Review X **7**, 031024 (2017).

[3] A. McDonald, R. Hanai, and A. A. Clerk, Nonequilibrium stationary states of quantum non-hermitian lattice models, Physical Review B **105**, 064302 (2022).

[4] P. Weinberg and M. Bukov, Quspin: a python package for dynamics and exact diagonalisation of quantum many body systems part i: spin chains, SciPost Physics **2**, 003 (2017).

[5] P. Weinberg and M. Bukov, Quspin: a python package for dynamics and exact diagonalisation of quantum many body systems. part ii: bosons, fermions and higher spins, SciPost Physics **7**, 020 (2019).

[6] B. Bauer, L. Carr, H. G. Evertz, A. Feiguin, J. Freire, S. Fuchs, L. Gamper, J. Gukelberger, E. Gull, S. Guertler, *et al.*, The alps project release 2.0: open source software for strongly correlated systems, Journal of Statistical Mechanics: Theory and Experiment **2011**, P05001 (2011).

[7] M. Dolfi, B. Bauer, S. Keller, A. Kosenkov, T. Ewart, A. Kantian, T. Giamarchi, and M. Troyer, Matrix product state applications for the alps project, Computer Physics Communications **185**, 3430 (2014).

[8] J. Gray, quimb: A python package for quantum information and many-body calculations, Journal of Open Source Software **3**, 819 (2018).

[9] D. Kochkov, *On numerical methods in quantum spin systems*, Ph.D. thesis, University of Illinois at Urbana-Champaign (2019).

[10] D. Kouzoudis, Heisenberg s= 12 ring consisting of a prime number of atoms, Journal of magnetism and magnetic materials **173**, 259 (1997).

[11] J.-H. Jung and J. D. Noh, Guide to exact diagonalization study of quantum thermalization, Journal of the Korean Physical Society **76**, 670 (2020).

[12] K. Adegoke and H. Büttner, Symmetry considerations and the exact diagonalization of finite spin systems, Chinese Journal of Physics **48**, 493 (2010).

[13] K. Bärwinkel, H.-J. Schmidt, and J. Schnack, Structure and relevant dimension of the heisenberg model and applications to spin rings, Journal of magnetism and magnetic materials **212**, 240 (2000).

[14] E. Cortese, L. Garziano, and S. De Liberato, Polariton spectrum of the dicke-ising model, Physical Review A **96**, 053861 (2017).

[15] J. K. Asbóth, L. Oroszlány, and A. Pályi, A short course on topological insulators, Lecture notes in physics **919**, 166 (2016).

[16] W. Dobrautz, Development of full configuration interaction quantum monte carlo methods for strongly correlated electron systems, (2019).

[17] W. A. Benalcazar, B. A. Bernevig, and T. L. Hughes, Quantized electric multipole insulators, Science **357**, 61 (2017).

[18] M. Mochol-Grzelak, A. Dauphin, A. Celi, and M. Lewenstein, Efficient algorithm to compute the second chern number in four dimensional systems, Quantum Science and Technology **4**, 014009 (2018).

[19] D. J. Thouless, M. Kohmoto, M. P. Nightingale, and M. den Nijs, Quantized hall conductance in a two-dimensional periodic potential, Physical review letters **49**, 405 (1982).

[20] M. Nakahara, Graduate student series in physics, Geometry, Topology and Physics, Second Edition (Taylor & Francis, 2003) (2003).

[21] J. Zhong, K. Wang, Y. Park, V. Asadchy, C. C. Wojcik, A. Dutt, and S. Fan, Nontrivial point-gap topology and non-hermitian skin effect in photonic crystals, Physical Review B **104**, 125416 (2021).

[22] Z. Gong, Y. Ashida, K. Kawabata, K. Takasan, S. Higashikawa, and M. Ueda, Topological phases of non-hermitian systems, Physical Review X **8**, 031079 (2018).

[23] A. McDonald, T. Pereg-Barnea, and A. Clerk, Phase-dependent chiral transport and effective non-hermitian dynamics in a bosonic kitaev-majorana chain, Physical Review X **8**, 041031 (2018).

[24] M. S. Rudner and L. Levitov, Topological transition in a non-hermitian quantum walk, Physical review letters **102**, 065703 (2009).

[25] H. Hu and E. Zhao, Knots and non-hermitian bloch bands, Physical Review Letters **126**, 010401 (2021).

[26] S. J. Masson, I. Ferrier-Barbut, L. A. Orozco, A. Browaeys, and A. Asenjo-Garcia, Many-body signatures of collective decay in atomic chains, Physical review letters **125**, 263601 (2020).

[27] S. J. Masson and A. Asenjo-Garcia, Universality of dicke superradiance in arrays of quantum emitters, Nature Communications **13**, 1 (2022).

[28] T. L. Patti, D. S. Wild, E. Shahmoon, M. D. Lukin, and S. F. Yelin, Controlling interactions between quantum emitters using atom arrays, Physical review letters **126**, 223602 (2021).

[29] S. Buckley-Bonanno, S. Ostermann, O. Rubies-Bigorda, T. L. Patti, and S. F. Yelin, Optimized geometries for cooperative photon storage in an impurity coupled to a two-dimensional atomic array, Physical Review A **106**, 053706 (2022).

[30] C. W. Gardiner and M. J. Collett, Input and output in damped quantum systems: Quantum stochastic differential equations and the master equation, Physical Review A **31**, 3761 (1985).

[31] A. Clerk, Introduction to quantum non-reciprocal interactions: from non-hermitian hamiltonians to quantum master equations and quantum feedforward schemes, SciPost Physics Lecture Notes , 044 (2022).

[32] M. Assunção, G. Diniz, L. Sanz, and F. Souza, Autler-townes doublet observation via a cooper-pair beam splitter, Physical Review B **98**, 075423 (2018).

[33] C. E. Granade, Characterization, verification and control for large quantum systems, (2015).

[34] R. Piil and K. Mølmer, Tunneling couplings in discrete lattices, single-particle band structure, and eigenstates of interacting atom pairs, Physical Review A **76**, 023607 (2007).

[35] Z. Wang, T. Jaako, P. Kirton, and P. Rabl, Supercorrelated radiance in nonlinear photonic waveguides, Physical Review Letters **124**, 213601 (2020).
[36] J. Talukdar and D. Blume, Undamped rabi oscillations due to polaron-emitter hybrid states in a nonlinear photonic waveguide coupled to emitters, Physical Review A **106**, 013722 (2022).
[37] R. El-Ganainy, K. G. Makris, M. Khajavikhan, Z. H. Musslimani, S. Rotter, and D. N. Christodoulides, Non-hermitian physics and pt symmetry, Nature Physics **14**, 11 (2018).
[38] Ş. K. Özdemir, S. Rotter, F. Nori, and L. Yang, Parity–time symmetry and exceptional points in photonics, Nature materials **18**, 783 (2019).
[39] Q. Wang and Y. Chong, Non-hermitian photonic lattices: tutorial, arXiv preprint arXiv:2212.00307 (2022).
[40] H. Xue, Q. Wang, B. Zhang, and Y. Chong, Non-hermitian dirac cones, Physical Review Letters **124**, 236403 (2020).
[41] H. Shen, B. Zhen, and L. Fu, Topological band theory for non-hermitian hamiltonians, Physical review letters **120**, 146402 (2018).
[42] S. Yao, F. Song, and Z. Wang, Non-hermitian chern bands, Physical review letters **121**, 136802 (2018).
[43] D. C. Brody, Biorthogonal quantum mechanics, Journal of Physics A: Mathematical and Theoretical **47**, 035305 (2013).
[44] S.-D. Liang and G.-Y. Huang, Topological invariance and global berry phase in non-hermitian systems, Physical Review A **87**, 012118 (2013).
[45] X.-L. Qi, Y.-S. Wu, and S.-C. Zhang, Topological quantization of the spin hall effect in two-dimensional paramagnetic semiconductors, Physical Review B **74**, 085308 (2006).
[46] F. H. Essler, H. Frahm, F. Göhmann, A. Klümper, and V. E. Korepin, *The one-dimensional Hubbard model* (Cambridge University Press, 2005).
[47] B. Paredes and J. I. Cirac, From cooper pairs to luttinger liquids with bosonic atoms in optical lattices, Physical review letters **90**, 150402 (2003).
[48] D. Jaksch, C. Bruder, J. I. Cirac, C. W. Gardiner, and P. Zoller, Cold bosonic atoms in optical lattices, Physical Review Letters **81**, 3108 (1998).
[49] O. Cherbal and M. Drir, Dissipative two-level spin system and geometrical phase, IIb **1**, 0 (2006).
[50] A. W. Sandvik, Computational studies of quantum spin systems, in *AIP Conference Proceedings*, Vol. 1297 (American Institute of Physics, 2010) pp. 135–338.